from merged status) for fibronectin complexed DOTAP-apatite particles in comparision with the uncomplexed one (Fig. 4C, lower panel). This result, is again suggesting that the receptor mediated endocytosis might caused enhanced mRNA internalization through fibronectin complexed carrier and better level of co localized mRNA within a single cell in compared to the uncomplexed one.

Analysis of the Expression Pattern of Fibronectin Coated Particles We then examined the effect of fibronectin on the trasfection efficiency of DOTAP-apatite particles by checking the gene expression pattern in HeLa cell. As stated previously that optimum concentration of DOTAP was determined for a certain amount of luiciferase mRNA in HeLa cell by applying 4 to 16 μg of DOTAP along with 3 μg of Luc-mRNA to form either mRNA-DOTAP complex or mRNA-DOTAP-apatite complex.[5] Then mRNA-DOTAP-apatite-Fn complexes were formed using 2—50 μg/mL fibronectin and all the complexes were then allowed to transfect HeLa cells. Luciferase expression was determined at 6 h post transfection. The expression has been enhanced around 2 times due to the presence of fibronectin on the DOTAP-apatite particles as shown in Fig. 5A. Among the different concentrations, 2 μg/mL fibronectin showed maximum enhancement, then exhibited gradual decrease as concentration of fibronectin increases (Fig. 5A). Many parameters including size of delivery particles are known to influence transfection efficiency and larger particles are more efficient in transfection.[33,34] Thus this strategy of decreasing efficiency with increasing Fn concentration can be correlated with size of the particles. As size decreased for increasing fibronectin concentration, larger complexes with lower fibronectin value (2 μg/mL) exhibited maximum enhancement of the expression (Fig. 5A). On the other hand, even though bigger, DOTAP-apatite paricles had lower efficiency than the fibronectin complexed one due to better association with the cell. It is noteworthy that Fn-DOTAP-apatite particles showed more than 50 times enhanced transfection potency than the only DOTAP (the so far reported most efficient non-viral mRNA carrier). This result shows a potential way to significantly improve mRNA transfection potency over the existing liposome technology.

Fibronectin is a large (440 kDa) multidomain extracellular matrix protein with an RGD site that is not exposed in its native compact conformation. When complexed with liposome vector, fibronectin adopts a conformation that is more open than its compact conformation.[35] This open conformation exposes a hidden RGD site in Fn that stimulates binding to adhesion molecules. In our investigation, the hidden RGD site of the fibronectin coated complex might be exposed.

Proof of Integrin-Mediated Delivery and Expression To evaluate one of the possible reasons for Fn-DOTAP-apatite mediated trans-gene delivery and expression we performed an inhibition assay adding excess amount of free (200 μg/mL) fibronectin to the preformed particle suspension, and incubated the cell for the same period of time as followed in usual transfection procedure. Decrease in mRNA transfection potency (Fig. 5B) indicated competitive blocking of the specific integrin receptors by free fibronectin might diminished interaction between Fn-DOTAP-apatite particles with cell membrane thus decreasing uptake and further expression too.

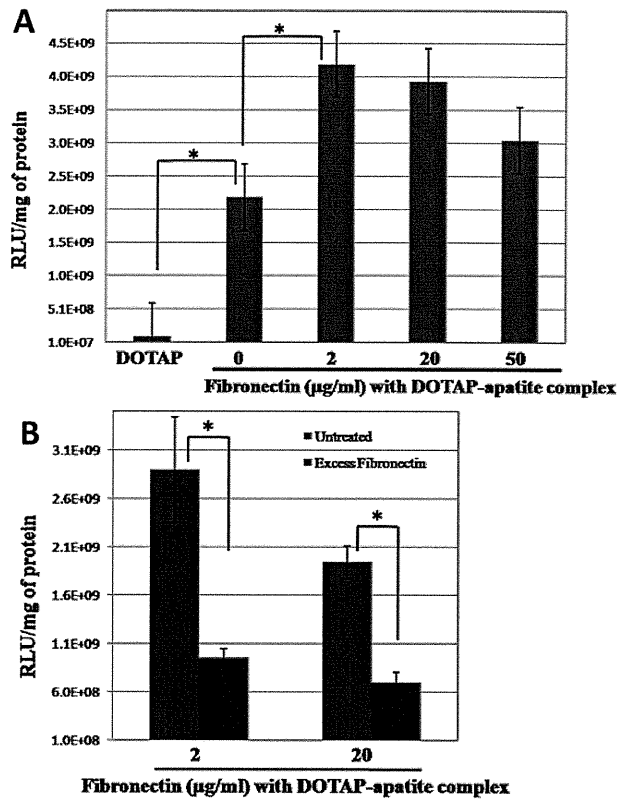

Fig. 5. Gene Expression Pattern by Fibronectin Coated DOTAP-Apatite Particles and Competitive Inhibition Assay

mRNA-DOTAP and fibronectin (2 μg/mL) coated or uncoated mRNA-DOTAP-apatite complexes were prepared as described in the text. Complexes were transferred with 10% FBS to 80% confluent HeLa cells seeded in 24 well plate and incubated for 3 h (A). After the addition of 10% FBS into the complex containing solution, excess fibronectin (200 μg/mL)was added and then the whole solution was added to 80% confluent HeLa cells seeded in 24 well plate (B). Luciferase mRNA expression was measured at 6 h post transfection. Luciferase activity was measured as RLU/mg of protein. * indicates $p<0.05$ *versus* untreated control.

CONCLUSION

Simple fabrication to attain improved tranfection potency is one of the important criteria for designing a better carrier. We could fabricate our developed mRNA carrier with the cell recognizable protein like fibronectin. This is the first time report of inorganic-organic hybrid mRNA carrier by ECM protein. Thus, we have established a superior mRNA transfection methodology based on anchoring liposome bound nano-apatite particles with the ECM protein that possibly could effectively associate with the cell membrane allowing better internalization and subsequent expression.

Acknowledgment This work was supported in parts by Grants-in-Aid for Scientific Research from the Ministry of Education, Culture, Sports, Science and Technology of Japan.

REFERENCES

1) Zou S, Scarfo K, Nantz MH, Hecker JG. Lipid-mediated delivery of RNA is more efficient than delivery of DNA in non-dividing cells. *Int. J. Pharm.*, **389**, 232—243 (2010).
2) Rejman J, Tavernier G, Bavarsad N, Demeester J, De Smedt SC.

mRNA transfection of cervical carcinoma and mesenchymal stem cells mediated by cationic carriers. *J. Control. Release*, **147**, 385—391 (2010).
3) Zohra FT, Chowdhury EH, Akaike T. High performance mRNA transfection through carbonate apatite-cationic liposome conjugates. *Biomaterials*, **30**, 4006—4013 (2009).
4) Zohra FT, Chowdhury EH, Tada S, Hoshiba T, Akaike T. Effective delivery with enhanced translational activity synergistically accelerates mRNA-based transfection. *Biochem. Biophys. Res. Commun.*, **358**, 373—378 (2007).
5) Zohra FT, Chowdhury EH, Nagaoka M, Akaike T. Drastic effect of nanoapatite particles on liposome-mediated mRNA delivery to mammalian cells. *Anal. Biochem.*, **345**, 164—166 (2005).
6) Bettinger T, Carlisle RC, Read ML, Ogris M, Seymour LW. Peptide-mediated RNA delivery: a novel approach for enhanced transfection of primary and post-mitotic cells. *Nucleic Acids Res.*, **29**, 3882—3891 (2001).
7) Karikó K, Kuo A, Barnathan E. Overexpression of urokinase receptor in mammalian cells following administration of the *in vitro* transcribed encoding mRNA. *Gene Ther.*, **6**, 1092—1100 (1999).
8) Pollard H, Remy JS, Loussouarn G, Demolombe S, Behr JP, Escande D. Polyethylenimine but not cationic lipids promotes transgene delivery to the nucleus in mammalian cells. *J. Biol. Chem.*, **273**, 7507—7511 (1998).
9) Brunner S, Sauer T, Carotta S, Cotten M, Saltik M, Wagner E. Cell cycle dependence of gene transfer by lipoplex, polyplex and recombinant adenovirus. *Gene Ther.*, **7**, 401—407 (2000).
10) Yew NS, Wang KX, Przybylska M, Bagley RG, Stedman M, Marshall J, Scheule RK, Cheng SH. Contribution of plasmid DNA to inflammation in the lung after administration of cationic lipid:pDNA complexes. *Hum. Gene Ther.*, **10**, 223—234 (1999).
11) Yew NS, Zhao H, Wu IH, Song A, Tousignant JD, Przybylska M, Cheng SH. Reduced inflammatory response to plasmid DNA vectors by elimination and inhibition of immunostimulatory CpG motifs. *Mol. Ther.*, **1**, 255—262 (2000).
12) Anderson DM, Hall LL, Ayyalapu AR, Irion VR, Nantz MH, Hecker JG. Stability of mRNA/cationic lipid lipoplexes in human and rat cerebrospinal fluid: methods and evidence for nonviral mRNA gene delivery to the central nervous system. *Hum. Gene Ther.*, **14**, 191—202 (2003).
13) Hecker JG, Hall LL, Irion VR. Nonviral gene delivery to the lateral ventricles in rat brain: initial evidence for widespread distribution and expression in the central nervous system. *Mol. Ther.*, **3**, 375—384 (2001).
14) Mitchell DA, Nair SK. RNA transfected dendritic cells as cancer vaccines. *Curr. Opin. Mol. Ther.*, **2**, 176—181 (2000).
15) Kyte JA, Kvalheim G, Aamdal S, Saebøe-Larssen S, Gaudernack G. Preclinical full-scale evaluation of dendritic cells transfected with autologous tumor-mRNA for melanoma vaccination. *Cancer Gene Ther.*, **12**, 579—591 (2005).
16) Zhang HM, Zhang LW, Ren J, Fan L, Si XM, Liu WC. Induction of α-fetoprotein-specific CD4- and CD8-mediated T-cell response using RNA-transfected dendritic cells. *Cell. Immunol.*, **239**, 144—150 (2006).
17) Qiu J, Lil GW, Sui YF, Sun YJ, Huang YY, Si SY, Ge W, Song HP. TruncatedTERT mRNA transfected dendritic cells evoke TERT specific antitumor response *in vivo*. *Hepatogastroenterology*, **54**, 681—687 (2007).
18) Kyte JA, Gaudernack G. Immuno-gene therapy of cancer with tumour-mRNA transfected dendritic cells. *Cancer Immunol. Immunother.*, **55**, 1432—1442 (2006).
19) Weide B, Pascolo S, Scheel B, Derhovanessian E, Pflugfelder A, Eigentler TK, Pawelec G, Hoerr I, Rammensee HG, Garbe C. Direct injection of protamine-protected mRNA: results of a phase 1/2 vaccination trial in metastatic melanoma patients. *J. Immunother.*, **32**, 498—507 (2009).
20) Romanov VI, Goligorsky MS. RGD-recognizing integrins mediate interactions of human prostate carcinoma cells with endothelial cells *in vitro*. *Prostate*, **39**, 108—118 (1999).
21) Anwer K, Kao G, Rolland A, Driessen WH, Sullivan SM. Peptide-mediated gene transfer of cationic lipid/plasmid DNA complexes to endothelial cells. *J. Drug Target.*, **12**, 215—221 (2004).
22) Harvie P, Dutzar B, Galbraith T, Cudmore S, O'Mahony D, Anklesaria P, Paul R. Targeting of lipid-protamine-DNA (LPD) lipopolyplexes using RGD motifs. *J. Liposome Res.*, **13**, 231—247 (2003).
23) Schiffelers RM, Ansari A, Xu J, Zhou Q, Tang Q, Storm G, Molema G, Lu PY, Scaria PV, Woodle MC. Cancer siRNA therapy by tumor selective delivery with ligand-targeted sterically stabilized nanoparticle. *Nucleic Acids Res.*, **32**, e149 (2004).
24) Kunath K, Merdan T, Hegener O, Häberlein H, Kissel T. Integrin targeting using RGD-PEI conjugates for *in vitro* gene transfer. *J. Gene Med.*, **5**, 588—599 (2003).
25) Jenkins RG, Meng QH, Hodges RJ, Lee LK, Bottoms SE, Laurent GJ, Willis D, Ayazi Shamlou P, McAnulty RJ, Hart SL. Formation of LID vector complexes in water alters physicochemical properties and enhances pulmonary gene expression *in vivo*. *Gene Ther.*, **10**, 1026—1034 (2003).
26) Hart SL, Arancibia-Cárcamo CV, Wolfert MA, Mailhos C, O'Reilly NJ, Ali RR, Coutelle C, George AJ, Harbottle RP, Knight AM, Larkin DF, Levinsky RJ, Seymour LW, Thrasher AJ, Kinnon C. Lipid-mediated enhancement of transfection by a nonviral integrin-targeting vector. *Hum. Gene Ther.*, **9**, 575—585 (1998).
27) Takita K, Ohsaki Y, Nakata M, Kurisu K. Immunofluorescence localization of type I and type III collagen and fibronectin in mouse dental tissues in late development and during molar eruption. *Arch. Oral Biol.*, **32**, 273—279 (1987).
28) Pearson BS, Klebe RJ, Boyan BD, Moskowicz D. Comments on the clinical application of fibronectin in dentistry. *J. Dent. Res.*, **67**, 515—517 (1988).
29) Wu TJ, Huang HH, Lan CW, Lin CH, Hsu FY, Wang YJ. Studies on the microspheres comprised of reconstituted collagen and hydroxyapatite. *Biomaterials*, **25**, 651—658 (2004).
30) Reyes CD, García AJ. Alpha2betal integrin-specific collagen-mimetic surfaces supporting osteoblastic differentiation. *J. Biomed. Mater. Res. A*, **69**, 591—600 (2004).
31) Shigeyama Y, Grove TK, Strayhorn C, Somerman MJ. Expression of adhesion molecules during tooth resorption in feline teeth: a model system for aggressive osteoclastic activity. *J. Dent. Res.*, **75**, 1650—1657 (1996).
32) Chowdhury EH, Nagaoka M, Ogiwara K, Zohra FT, Kutsuzawa K, Tada S, Kitamura C, Akaike T. Integrin-supported fast rate intracellular delivery of plasmid DNA by extracellular matrix protein embedded calcium phosphate complexes. *Biochemistry*, **44**, 12273—12278 (2005).
33) Almofti MR, Harashima H, Shinohara Y, Almofti A, Li W, Kiwada H. Lipoplex size determines lipofection efficiency with or without serum. *Mol. Membr. Biol.*, **20**, 35—43 (2003).
34) Escriou V, Ciolina C, Lacroix F, Byk G, Scherman D, Wils P. Cationic lipid-mediated gene transfer: effect of serum on cellular uptake and intracellular fate of lipopolyamine/DNA complexes. *Biochim. Biophys. Acta*, **1368**, 276—288 (1998).
35) Halter M, Antia M, Vogel V. Fibronectin conformational changes induced by adsorption to liposomes. *J. Control. Release*, **101**, 209—222 (2005).

Antitumor Effect of Liposomal Histone Deacetylase Inhibitor-Lipid Conjugates *in Vitro*

Yoshiyuki HATTORI,*[,a] Yasuo NAGAOKA,[b] Manami KUBO,[a] Haruka YAMASAKU,[a] Yuta ISHII,[b] Hiroko OKITA,[b] Hiroki NAKANO,[b] Shinichi UESATO,[b] and Yoshie MAITANI[a]

[a] *Institute of Medicinal Chemistry, Hoshi University; 2–4–41 Ebara, Shinagawa-ku, Tokyo 142–8501, Japan: and* [b] *Faculty of Chemistry, Materials and Bioengineering, Kansai University; Suita, Osaka 564–8680, Japan.*
Received August 2, 2011; accepted August 29, 2011; published online September 7, 2011

Histone deacetylase inhibitor (HDACI), suberoylanilide hydroxamic acid (SAHA), approved by the Food and Drug Administration (FDA) for the treatment of cutaneous T cell lymphoma, is a promising new treatment strategy for various cancers. In this study, we hypothesized that a liposomal formulation of HDACI might efficiently deliver HDACI into tumors. To incorporate HDACI efficiently into the liposomal membrane, we synthesized six HDACI-lipid conjugates, in which polyethylene glycol$_{2000}$ (PEG$_{2000}$)-lipid or cholesterol (Chol) was linked with a potent hydroxamic acid, HDACI, SAHA or K-182, by cleavable linkers, such as ester, carbamide and disulfide bonds. Liposomal HDACI-lipid conjugates were prepared with distearoylphosphatidylcholine (DSPC) and HDACI-Chol conjugate or with DSPC, Chol and HDACI-PEG-lipid conjugates, and their cytotoxicities were evaluated for human cervix tumor HeLa and mouse colon tumor Colon 26 cells. Among the liposomes, liposomal oleyl-PEG$_{2000}$-SAHA conjugated with SAHA and oleyl-PEG$_{2000}$ *via* a carbamate linker showed higher cytotoxicity *via* hyperacetylation of histone H3 and induction of caspase 3/7 activity. These results suggested that liposomal HDACI-lipid conjugates may be a potential tool for cancer therapy.

Key words histone deacetylase inhibitor; suberoylanilide hydroxamic acid; liposome; cytotoxicity

Histone deacetylases (HDAC) are a family of enzymes that have been identified as a promising target to reverse aberrant epigenetic states associated with cancer *via* the regulation of acetylation levels in histone.[1,2] Aberrant histone acetylation has been observed in the development of numerous malignancies, and HDAC inhibitors (HDACIs) are a promising new treatment strategy for malignant disease.[3] The hydroxamic acid trichostatin A (TSA) have been known as a differentiation inducer for tumor cells, but its clinical use has been limited by high reactivity and instability. Furthermore, TSA has also been reported to be unstable *in vivo* following intravenous injection in mice.[4,5]

Suberoylanilide hydroxamic acid (SAHA, vorinostat, Zolinza), is a potent HDACI that has demonstrated antitumor activity *in vitro* against a variety of cell lines and *in vivo* against several human tumor xenograft models.[6—8] Furthermore, SAHA is currently prescribed to treat cutaneous T-cell lymphoma[9] and is also being tested in several phase I to III clinical trials for the treatment of a variety of other cancers, including breast, lung, and colon.[10,11] Although SAHA is orally administrated because of its hydrophobic property, it is easily metabolized in the liver. Pharmacokinetic studies in patients after administration of SAHA have identified two inactive metabolites, SAHA-glucuronide and 4-anilino-4-oxobutanoic acid, which are pharmacologically inactive, and the mean terminal half-life ($t_{1/2}$) of SAHA was *ca.* 2.0 h[12,13]; therefore, the liposomal SAHA formulation warrants *in vivo* experiments because it allows intravenous administration and prevents metabolism in the liver.

Liposomes have the advantage of an enhanced permeability and retention effect (EPR), increasing their tumor accumulation when they are intravenously injected.[14] Such a type of nanocarrier is supposed to improve the pharmacokinetic and pharmacodistribution of the encapsulated drug. Liposomal LAQ824, hydrophilic hydroxamic acid HDACI, was shown to be both long-circulating and highly stable *in vivo*[14]; however, in the encapsulation of hydrophobic SAHA into liposome, SAHA must be incorporated into the lipid membrane, which might be limited in its capacity to entrap SAHA. We therefore attempted to synthesize hydroxamate-type HDACI-lipid conjugates as a component of the liposome formulation for efficient incorporation into the liposomal membrane. Previously, we have reported that inclusion of HDACI-lipid conjugates into cationic nanopartilces as a non-viral vector could increase gene expression *via* hyper acetylation of histone.[15] In this study, taking into consideration the diverse derivatization, we selected SAHA and one of the K-series compounds, K-182, which has two OH groups to tether other groups with a biodegradable ester bond, and synthesized cholesteryl HDACI and HDACI-polyethylene glycol (PEG)-lipid conjugates to prepare liposomal HDACI-lipid conjugates (Fig. 1). Furthermore, we evaluated their cytotoxic effect on tumor cells *via* the acetylation of histone H3 and apoptotic activity.

Experimental

Synthesis of HDACI-Lipid Conjugates IR spectra were recorded on a Shimadzu FTIR-8400 infrared spectrophotometer. FAB-MS spectra were measured on a JEOL JMS-HX 100 instrument. ^{1}H- and ^{13}C-NMR spectra were recorded on JEOL EX-400 (399.7 MHz for ^{1}H-NMR and 100.4 MHz for ^{13}C-NMR) instruments using tetramethylsilane as an internal standard. Analytical and preparative TLC were performed using Silica gel 60 F254 (Merck, 0.25, 1 mm, respectively) glass plates. Column chromatography was performed using Silica Gel 60 (70—230 mesh ASTM). CM-K-182 was prepared according to the method described previously.[15]

Synthesis of Cholest-5-en-3-yl (2*R*)-2-{[(9*H*-Fluoren-9-ylmethoxy)carbonyl]amino}-3-{[(4-methoxyphenyl)(diphenyl)methyl]sulfanyl}-propanoate (2) A solution of Fmoc-Cys (Mmt) –OH (**1**) (500 mg, 0.81 mmol), cholesterol (314 mg, 0.81 mmol), dimethylaminopyridine (DMAP) (99 mg, 0.81 mmol) and dicyclohexylcarbodiimide (DCC) (178 mg, 0.81 mmol) in CH_2Cl_2 (3 ml) was stirred at room temperature for 3 h (Chart 1). After the removal of DCU by filtration, the solution was diluted with $CHCl_3$, washed with 0.1 M HCl, 5% $NaHCO_3$ and saturated NaCl and then dried over Na_2SO_4. Concentration and column chromatography (EtOAc/hexane=1/5) gave **2** (581 mg, 72.9%) as a colorless oil. IR (neat) cm^{-1}: 3428, 3028, 2951, 2855, 1728, 1669, 700. ^{1}H-NMR (399.65 MHz,

* To whom correspondence should be addressed. e-mail: yhattori@hoshi.ac.jp

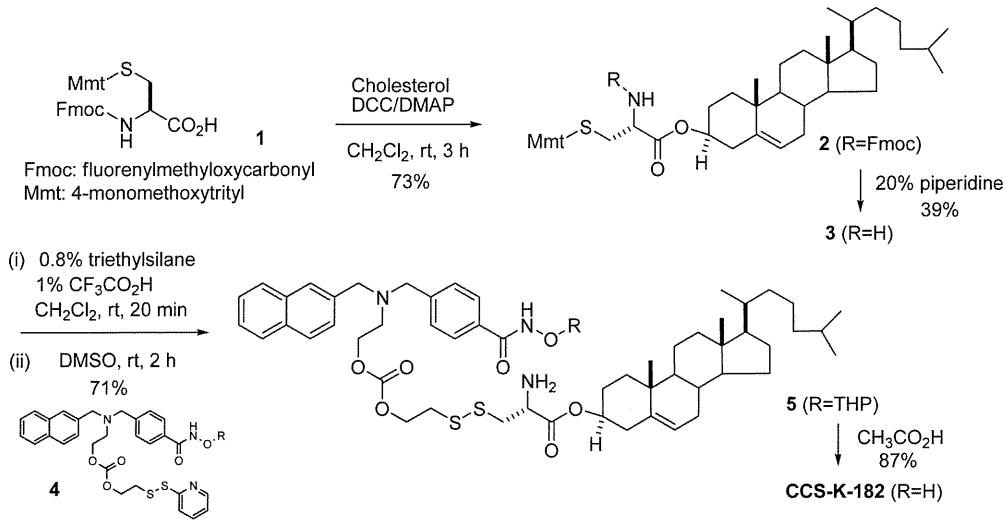

Chart 1. Synthesis Scheme for CCS-K-182

$CDCl_3$) δ: 0.68—2.04 (44H, m, chol), 2.30 (2H, m, S–CH_2–CH), 2.64 (1H, m, COO–CH), 3.76 (3H, s, O–CH_3), 4.24 (1H, m, CH_2–CH–$(Ar)_2$), 4.35 (2H, m, O–CH_2–CH), 4.63 (1H, m, NH_2–CH–COO), 5.32 (1H, m, CH_2–CH–C), 6.80—6.78 (2H, m, O–Ar–H), 7.18—7.77 (20H, m, Ar–H). ^{13}C-NMR (100.40 MHz, $CDCl_3$) δ: 11.85, 14.10, 18.70, 19.31, 21.02, 22.55, 22.64, 22.80, 23.82, 24.27, 27.64, 28.00, 28.21, 31.84, 31.89, 34.32, 35.78, 36.17, 36.55, 36.87, 37.84, 39.51, 39.71, 42.31, 47.09, 49.97, 53.05, 55.051, 56.13, 56.67, 66.44, 67.17, 75.66, 113.25, 119.95, 122.98, 125.15, 126.79, 127.08, 127.70, 127.97, 129.39, 129.42, 130.73, 136.40, 139.31, 141.26, 143.78, 143.91, 144.60, 144.64, 155.57, 158.21, 169.89. High resolution (HR)-FAB-MS *m/z*:1006.5414 (Calcd for $C_{65}H_{77}NNaO_5S$ [M+Na^+], 1006.5420).

Synthesis of Cholest-5-en-3-yl (2*R*)-2-Amino-3-{[(4-methoxyphenyl)-(diphenyl)methyl]sulfanyl}propanoate (3) A solution of **2** (330 mg, 0.34 mmol) in 20% piperidine/CH_2Cl_2 (4 ml) was stirred at room temperature for 20 min (Chart 1). The solution was diluted with $CHCl_3$, washed successively with water and saturated NaCl, and then dried over Na_2SO_4. Concentration and SiO_2 column chromatography (EtOAc/hexane=1/5) gave **3** (101 mg, 39% yield) as a colorless oil. IR (neat) cm^{-1}: 3400, 3050, 2951, 2855, 1718, 1650, 701; ^{1}H-NMR (399.65 MHz, $CDCl_3$) δ: 0.68—1.99 (43H, m, chol), 2.25 (2H, m, CH-CH_2-C=CH), 2.49 (2H, m, S–CH_2–CH), 3.20 (1H, t, J=8.6 Hz, NH_2–CH–COO), 3.78 (3H, s, O–CH_3), 4.52—4.60 (1H, m, O–CH), 5.36—5.36 (1H, m, CH_2–CH=C), 6.80—6.82 (2H, m, O–Ar–H), 7.20—7.43 (12H, m, Ar–H); ^{13}C-NMR (100.40 MHz $CDCl_3$) δ: 11.85, 14.19, 18.71, 19.31, 21.03, 22.54, 22.80, 23.83, 24.27, 27.65, 28.00, 28.21, 31.86, 31.89, 35.78, 36.18, 36.56, 36.91, 37.20, 37.93, 39.52, 39.72, 42.32, 50.01, 54.12, 55.20, 56.15, 56.68, 60.35, 66.37, 74.79, 113.18, 122.81, 126.66, 127.90, 129.51, 130.80, 136.66, 139.45, 144.91, 144.94, 158.16, 173.23; HR-FAB-MS *m/z*: 784.4734 (Calcd for $C_{50}H_{67}NNaO_3S$, 784.4739).

Synthesis of Cholest-5-en-3-yl (13*R*)-13-amino-1-(2-naphthyl)-6-oxo-2-(4-{[(tetrahydro-2*H*-pyran-2-yloxy)amino]carbonyl}benzyl)-5,7-dioxa-10,11-dithia-2-azatetradecan-14-oate (5) A solution of **3** (35.1 mg, 0.0462 mmol), trifluoroacetic acid (TFA) (16 μl), and triethylsilane (20 μl) in CH_2Cl_2 (2.0 ml) was stirred at 0 °C for 4 h under Ar atomosphere (Chart 1). After the solution was concentrated *in vacuo*, the residue was dissolved in dimethyl sulfoxide (DMSO) and to this was added **4**[15] (30 mg, 0.069 mmol). After stirring for another 2 h at room temperature, the solution was diluted with $CHCl_3$, washed with water and saturated NaCl, dried over Na_2SO_4 and concentrated. Purification with preparative SiO_2 thin layer chromatography (EtOAc/hexane=3/2) gave **5** (30 mg, 71% yield) as a colorless oil. IR (neat) cm^{-1}: 3400, 3030, 2935, 2855, 1734, 1684, 699. ^{1}H-NMR (399.65 MHz, $CDCl_3$) δ: 0.67—2.04 (53H, m), 2.31—2.33 (2H, d, J=7.6 Hz, SS–CH_2–CH), 2.81 (2H, t, J=8.4 Hz, N–CH_2–CH_2), 2.96 (2H, t, J=10.2 Hz, CH_2–CH_2–SS), 3.09—3.14 (1H, m, NH_2–CH–COO), 3.64 (2H, s, N–CH_2–Ar), 3.72 (2H, m, O–CH_2–CH_2), 3.80 (2H, s, Ar–CH_2–N), 4.25 (2H, t, J=8.4 Hz, CH_2–CH_2–OCOO), 4.36 (2H, t, J=9.6 Hz, OCOO–CH_2–CH_2), 4.64—4.67 (1H, m, O–CH), 5.07 (1H, m, O–CH–O), 5.30—5.36 (1H, d, J=23.6 Hz, CH_2–CH=C), 7.43—7.81 (11H, m, Ar–H); ^{13}C-NMR (100.40 MHz, $CDCl_3$) δ: 11.84, 18.70, 18.81, 19.28, 21.01, 22.54, 22.80, 23.81, 24.25, 25.04, 27.67, 27.99, 28.16, 28.20, 29.68, 31.82, 31.87, 35.76, 36.17, 36.55, 36.89. 37.99, 39.50, 39.70, 42.29, 49.98, 51.89, 53.82, 56.12, 56.66, 58.35, 58.95, 52.82, 65.61, 65.88, 75.28, 102.80, 122.96, 125.66, 126.02, 126.90, 127.25, 127.36, 127.66, 128.08, 128.87, 133.29, 136.34, 143.79, 154.90. HR-FAB-MS *m/z*: 1026.5697 (Calcd for $C_{59}H_{84}N_3O_8S_2$ [M+H^+], 1026.5700).

Synthesis of Cholest-5-en-3-yl (13*R*)-13-Amino-2-{4-[(hydroxyamino)-carbonyl]benzyl}-1-(2-naphthyl)-6-oxo-5,7-dioxa-10,11-dithia-2-aza-tetradecan-14-oate (CCS-K182) A mixture of **5** (20.0 mg, 0.0195 mmol) in CH_3CO_2H (0.8 ml), tetrahydrofuran (THF) (0.8 ml) and H_2O (0.2 ml) was stirred at 60 °C for 2.5 h (Chart 1). Concentration of the reaction mixture, followed by purification of the residue with preparative SiO_2 TLC (EtOAc) afforded CCS-K-182 (16 mg, 87% yield) as a colorless oil. IR (neat) cm^{-1}: 3400, 3019, 2930, 2855, 1740, 1650, 706. ^{1}H-NMR (399.65 MHz, $CDCl_3$) δ: 0.67—2.01 (47H, m), 2.31 (2H, m, SS–CH_2–CH), 2.77 (2H, m, N–CH_2–CH_2), 2.94 (2H, m, CH_2–CH_2–SS), 3.13 (1H, m, NH_2–CH–COO), 3.64 (2H, s, N–CH_2–Ar), 3.80 (2H, s, Ar–CH_2–N), 4.23 (2H, m, CH_2–CH_2–OCOO), 4.33 (2H, m, OCOO–CH_2–CH_2), 4.66 (1H, m, O–CH), 5.34 (1H, m, CH_2–CH=C), 7.44—7.82 (11H, m, Ar–H). ^{13}C-NMR (100.40 MHz $CDCl_3$) δ: 11.86, 14.13, 18.73, 19.30, 21.03, 22.57, 22.70, 22.82, 23.85, 24.28, 27.67, 28.02 28.22, 29.37, 29.70, 31.83, 31.89, 35.80, 36.20, 36.55, 36.89, 36.98, 37.99, 39.53, 39.72, 42.32, 49.98, 52.20, 56.15, 56.67, 58.34, 59.26, 65.65, 65.76, 70.53, 75.58, 123.02, 125.71, 126.07, 126.95, 127.43, 127.68, 128.15, 128.92, 132.86, 133.31, 136.35, 139.24, 144.03, 154.91. HR-FAB-MS *m/z*: 942.5115 (Calcd for $C_{54}H_{76}N_3O_7S_2$ [M+H^+], 942.5125).

Synthesis of 3-(2-Pyridinyldisulfanyl)propanoic Acid (7) 3-(2-Pyridinyldisulfanyl)propanoic acid (**7**) was synthesized according to the procedure described previously.[16] ^{1}H-NMR (399.65 MHz, $CDCl_3$) δ: 2.80 (2H, t, J=6.8 Hz), 3.07 (2H, t, J=6.8 Hz), 7.16 (1H, ddd, J=7.8, 5.2, 1.6 Hz), 7.64 (1H, dd, J=7.8, 1.6 Hz), 7.67 (1H, dt, J=7.8, 1.6 Hz), 8.48 (1H, dd, J=5.2, 1.6 Hz).

Synthesis of Distearoylphosphatidylethanolamine (DSPE)-PEG-3-(2-pyridyldithio)propanoate (8) To a solution of **7** (43 mg, 0.2 mmol) in CH_2Cl_2 (1 ml) was added *N*-hydroxysuccineimide (HOSu, 23 mg, 0.2 mmol) and (DCC, 41 mg, 0.2 mmol) at 0 °C and the mixture was stirred at room temperature for 6 h (Chart 2). After the removal of precipitates by filtration, DSPG-PEG-NH_2 (50 mg, *ca.* 17.4 μmol) was added to the solution and stirred for another 18 h under the same conditions. The reaction mixture was concentrated, applied to Sephadex LH-20 gel filtration column chromatography (1.5 cm i.d.×45 cm) and eluted with methanol. The fractions of the eluate from 27 to 32 ml were collected and evaporated *in vacuo* to gave **8** (29 mg, *ca.* 9.4 μmol) as a colorless oil. Molecular weights of the components were calculated from electrospray ionization (ESI)-MS (+) multiply charged ion peaks for 2806 (*m/z* 936 (M+3H^+), 562 (M+5H^+)), 2850 (*m/z* 951 (M+3H^+), 713 (M+4H^+)), 2894 (*m/z* 966 (M+3H^+), 724 (M+4H^+), 579 (M+5H^+)), 3026 (*m/z* 1009 (M+3H^+), 757 (M+4H^+), 606 (M+5H^+)), 3114 (*m/z* 1039 (M+3H^+), 757 (M+4H^+), 624 (M+5H^+)), 3158 (*m/z* 1054 (M+3H^+), 790 (M+4H^+)), 3202 (*m/z* 1068 (M+3H^+), 641 (M+5H^+)) and 3246 (*m/z* 1083 (M+3H^+), 650 (M+5H^+)), These values corresponded to a

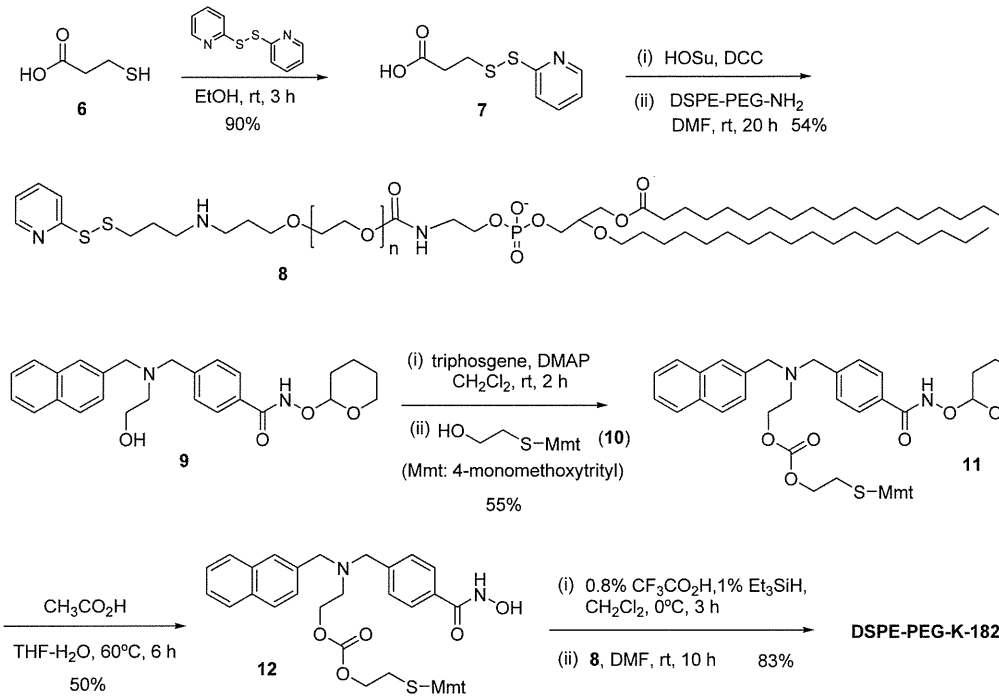

Chart 2. Synthesis Scheme for DSPE-PEG-K-182

mass number of **8**, whose polymerization degrees of PEG were from 40 to 50.

Synthesis of 2-{[(4-Methoxyphenyl)(diphenyl)methyl]sulfanyl}ethanol (10) To a solution of 4-methoxy triphenyl methyl chloride (2.00 g, 6.4 mmol) in *N,N*-dimethylformamide (DMF) (12 ml) was added 2-mercaptoethanol (0.45 ml, 6.4 mmol) and triethylamine (0.90 ml, 6.4 mmol) and the solution was stirred at room temperature for 3 h (Chart 2). After the addition of $CHCl_3$ (30 ml), the organic layer was washed with water (30 ml) and then dried over Na_2SO_4. Concentration and silica gel column chromatography (EtOAc/toluene=5/1) gave **10** (2.30 g, 70%) as yellow crystals. IR (neat) cm^{-1} 3590, 1722, 1602, 1506, 1250; ^{1}H-NMR (399.65 MHz, $CDCl_3$) δ: 2.40 (2H, t, J=6.0 Hz), 3.31 (2H, t, J=6.0 Hz), 3.74 (3H, s), 6.73 (2H, d, J=8.4 Hz), 7.1—7.5 (12H, m); ^{13}C-NMR (100.40 MHz $CDCl_3$) δ: 35.2, 55.2, 60.8, 66.1, 113.1, 126.7, 127.9, 129.4, 130.7, 136.8, 145.0, 158.1; HR-FAB-MS *m/z*: 351.1416 (Calcd for $C_{22}H_{23}O_2S$ $[M+H^+]$, 351.1419).

Synthesis of 2-{[(4-Methoxyphenyl)(diphenyl)methyl]sulfanyl}ethyl 2-[(2-Naphthylmethyl)(4-{[(tetrahydro-2*H*-pyran-2-yloxy)amino]carbonbenzyl)amino]ethyl Carbonate (11) To a solution of **9**[15] (100 mg, 0.23 mmol) and DMAP (169 mg, 1.38 mmol) in CH_2Cl_2 (2.00 ml) was added triphosgene (24 mg, 0.081 mmol) (Chart 2). After stirring at room temperature for 15 min, **10** (80.6 mg, 0.23 mmol) was added and the solution was stirred for another 7 h under the same conditions. The reaction mixture was diluted with $CHCl_3$, washed with water, and then dried over Na_2SO_4. Concentration and preparative thin layer silica gel chromatography (EtOAc/hexane=3/2) gave **11** (102 mg, 55%) as a brownish oil. IR (neat) cm^{-1} 3406, 3026, 2837, 1732, 1685; ^{1}H-NMR (399.65 MHz, $CDCl_3$) δ: 1.60—1.87 (6H, m, $3CH_2$ of THP), 2.51 (2H, t, J=6.0 Hz, CH_2–CH_2–S), 2.77 (2H, m, N–CH_2–CH_2), 3.65 (1H, m, O–CH_a–CH_2 of THP), 3.70 (2H, s, N–CH_2–Ar), 3.76 (3H, s, O–CH_3), 3.76 (2H, s, Ar–CH_2–N), 3.86 (2H, t, J=6.0 Hz, COO–CH_2–CH_2), 3.98 (1H, m, O–CH_b–CH_2 of THP), 4.19 (2H, t, J=5.2 Hz, CH_2–CH_2–OCOO), 5.06 (1H, m, O–CH–O), 6.79 (2H, d, J=8.0 Hz, Ar–H), 6.18—7.78 (13H, m, Ar–H); ^{13}C-NMR (100.40 MHz $CDCl_3$) δ: 18.64, 25.01, 28.05, 29.80, 30.63, 51.75, 55.20, 58.31, 58.81, 62.66, 65.71, 66.11, 66.45, 102.69, 113.20, 125.61, 125.99, 126.73, 126.86, 127.21, 127.33, 127.65, 127.94, 128.06, 128.90, 129.42, 130.76, 132.78, 133.25, 136.36, 136.54, 143.87, 144.81, 154.73, 158.13, 166.05; HR-FAB-MS *m/z*: 811.3425 (Calcd for $C_{49}H_{51}N_2O_7S$ $[M+H^+]$, 811.3417).

Synthesis of 2-[{4-[(Hydroxyamino)carbonyl]benzyl}(2-naphthylmethyl)amino]ethyl 2-{[(4-Methoxyphenyl)(diphenyl)methyl]sulfanyl}-ethyl Carbonate (12) A mixture of **11** (90 mg, 0.11 mmol) in CH_3CO_2H (0.8 ml), THF (0.4 ml) and H_2O (0.2 ml) was stirred at 60 °C for 6 h (Chart 2). After concentration of the reaction mixture, the resulting crude oil was applied to preparative SiO_2 thin layer chromatography (EtOAc/hexane=1/1) for separation to give **12** (80.6 mg, 50%) as a brownish oil. IR (neat) cm^{-1} 3400, 3030, 2837, 1741, 1660; ^{1}H-NMR (399.65 MHz, $CDCl_3$) δ: 2.50 (2H, m, CH_2–CH_2–STmt), 2.74 (2H, m, N–CH_2–CH_2), 3.51—4.00 (9H, m, Ar–CH_2–N, N–CH_2–Ar, COO–CH_2–CH_2, O–CH_3), 4.12 (2H, t, J=6.0 Hz, CH_2–CH_2–OCOO), 6.80—7.77 (15H, m, Ar–H); ^{13}C-NMR (100.40 MHz $CDCl_3$) δ: 29.65, 30.67, 51.75, 55.22, 58.23, 58.80, 65.67, 66.15, 66.45, 113.22, 125.61, 125.99, 126.73, 126.86, 127.31, 127.62, 126.86, 127.31, 127.62, 127.94, 129.40, 130.74, 132.76, 133.23, 136.52, 144.79, 154.72, 158.11, 171.20; HR-FAB-MS *m/z*: 727.2855 (Calcd for $C_{44}H_{43}N_2O_6S$ $[M+H^+]$, 727.2842).

Synthesis of DSPE-PEG-K-182 To a solution of **12** (30 mg, 0.039 mmol) in CH_2Cl_2 (2.0 ml) was added CF_3CO_2H (16 μl) and Et_3SiH (20 μl) and the solution was stirred at 0 °C for 4 h (Chart 2). After confirmation of the complete deprotection of the *p*-methoxytrityl group by TLC, the solution was evaporated to remove the solvent and regents. The residual oily mixture was applied to **8** (29 mg, *ca.* 9.4 μml) in DMF (0.5 ml) and the solution was stirred for another 20 h at room temperature. The resulting mixture was applied to Sephadex LH-20 column chromatography (1.5 cm i.d.×45 cm), eluted with methanol, and the eluate was between 20 and 26 ml, in which compounds with an average molecular weight were collected. Evaporation of the solvent gave DSPE-PEG-K-182 (25 mg, *ca.* 7.8 μmol) as a brownish oil. Molecular weight of the components was calculated from ESI-MS (+) multiply charged ion peaks for 3192 (*m/z* 1065 $(M+3H^+)$, 799 $(M+4H^+)$, 640 $(M+5H^+)$), 3237 (*m/z* 1080 $(M+3H^+)$, 810 $(M+4H^+)$, 648 $(M+5H^+)$), 3325 (*m/z* 1109 $(M+3H^+)$, 832 $(M+4H^+)$, 666 $(M+5H^+)$), 3369 (*m/z* 1124 $(M+3H^+)$, 843 $(M+4H^+)$, 675 $(M+5H^+)$), 3545 (*m/z* 1183 $(M+3H^+)$, 887 $(M+4H^+)$, 710 $(M+5H^+)$) and 3589 (*m/z* 1197 $(M+3H^+)$, 898 $(M+4H^+)$, 719 $(M+5H^+)$). These values corresponded to the mass number of DSPE-PEG-K-182, whose polymerization degrees of PEG were from 40 to 50.

Synthesis of DSPE-PEG-SAHA To a solution of SAHA[17] (26 mg, 98 μmol) in DMF (0.3 ml) was added 3-(*N*-succinimidyloxyglutaryl)amino-propyl, polyethyleneglycol-carbamyldistearoylphosphatidyl-ethanolamine (DSPE-PEG-NHS) (30 mg, *ca.* 9.8 μmol) and the solution was stirred at room temperature for 12 h. After concentration of the reaction mixture, the residue was applied to Sephadex LH-20 gel filtration column chromatography (1.5 cm i.d.×45 cm) and eluted with methanol. The fractions of the eluate from 20 to 28 ml were collected and evaporated *in vacuo* to gave DSPE-PEG-SAHA (21 mg, *ca.* 9.4 μmol) as a colorless oil. Molecular weights of the components were calculated from ESI-MS (+) multiply charged ion peaks for 2806 (*m/z* 936 $(M+3H^+)$, 562 $(M+5H^+)$), 2850 (*m/z* 951 $(M+3H^+)$, 713 $(M+4H^+)$), 2894 (*m/z* 966 $(M+3H^+)$, 724 $(M+4H^+)$, 579

($M+5H^+$)), 3026 (*m/z* 1009 ($M+3H^+$), 757 ($M+4H^+$), 606 ($M+5H^+$)), 3114 (*m/z* 1039 ($M+3H^+$), 757 ($M+4H^+$), 624 ($M+5H^+$)), 3158 (*m/z* 1054 ($M+3H^+$), 790 ($M+4H^+$)), 3202 (*m/z* 1068 ($M+3H^+$), 641 ($M+5H^+$)) and 3246 (*m/z* 1083 ($M+3H^+$), 650 ($M+5H^+$)), These values corresponded to a molecular weight of 13, whose polymerization degrees of PEG were from 40 to 50.

Synthesis of Oleyl-PEG-SAHA To a solution of SAHA[17] (63 mg, 0.24 mmol) in DMF (3 ml) was added oleyl-PEG-NHS (100 mg, *ca.* 0.041 mmol), which was stirred at room temperature for 20 h. After concentration of the reaction mixture, the residue was applied to Sephadex LH-20 gel filtration column chromatography (1.5 cm i.d.×45 cm) and eluted with methanol. The fractions of the eluate from 25 to 30 ml were collected and evaporated *in vacuo* to give oleyl-PEG-SAHA (OL-PEG-SAHA, 107 mg, *ca.* 0.040 mmol) as a colorless oil. Molecular weights of the components were calculated from ESI-MS (+) multiply charged ion peaks for 2022 (*m/z* 1012 ($M+2H^+$), 675 ($M+3H^+$)), 2066 (*m/z* 1034 ($M+2H^+$), 690 ($M+3H^+$)), 2110 (*m/z* 1056 ($M+2H^+$), 704 ($M+3H^+$)), 2154 (*m/z* 1078 ($M+2H^+$), 719 ($M+3H^+$)), 2198 (*m/z* 1100 ($M+2H^+$), 733 ($M+3H^+$)), 2242 (*m/z* 1122 ($M+2H^+$), 748 ($M+3H^+$)), 2286 (*m/z* 1144 ($M+2H^+$), 763 ($M+3H^+$)), 2330 (*m/z* 1166 ($M+2H^+$), 778 ($M+3H^+$), 583 ($M+4H^+$)), 2374 (*m/z* 1188 ($M+2H^+$), 792 ($M+3H^+$), 594 ($M+4H^+$)), 2418 (*m/z* 1210 ($M+2H^+$), 807 ($M+3H^+$), 605 ($M+4H^+$)), 2462 (*m/z* 1232 ($M+2H^+$), 822 ($M+3H^+$), 616 ($M+4H^+$)) and 2506 (*m/z* 1254 ($M+2H^+$), 866 ($M+3H^+$), 649 ($M+4H^+$)). These values corresponded to molecular weight of OL-PEG-SAHA, whose polymerization degrees of PEG were from 32 to 45.

Preparation of Liposomal HDACI-Lipid Conjugate Liposomes (L) were prepared from distearoylphosphatidylcholine (DSPC)/cholesterol (Chol) (55/45, molar ratio) by a modified ethanol injection method, as reported previously.[15] For preparation of liposomal cholesteryl HDACI, Chol of liposome (L) formulation was substituted with CCS-K-182, CM-K-182 or CM-SAHA (L-CCS-K-182, L-CM-K-182 and L-CM-SAHA, respectively) (Table 1). For liposomal HDACI-PEG-lipid conjugates, 5 mol% of OL-PEG_{2000}-SAHA, DSPE-PEG_{2000}-SAHA and DSPE-PEG_{2000}-K-182 were added to the formulation of L (L-OL-PEG-SAHA, L-DSPE-PEG-SAHA and L-DSPE-PEG-K-182, respectively) (Table 1). As a control of liposomal HDACI-PEG-lipid conjugates, 5 mol% PEG_{2000}-DSPE was added to the formulation of L (L-DSPE-PEG). The particle size distributions and the ζ-potentials were measured by the dynamic light scattering method and the electrophoresis light scattering method, respectively (ELS-Z2; Otsuka Electronics Co., Ltd., Osaka, Japan), at 25 °C after dispersion and dilution to an appropriate volume with water.

Entrapment Efficiency of HDACI-Lipid Conjugate into Liposome Unencapsulated SAHA-lipid conjugates were removed using a Sephadex G-50 column eluted with saline adjusted to pH 7.4. After purification, the concentration of phospholipid (DSPC) in liposome suspension was measured with the Phospholipids C-test Wako (Wako Pure Chemical Industries, Ltd.). The amount of SAHA-lipid conjugate in liposomes was quantified as its acid hydrolysate, intact SAHA. Quantification of SAHA in the sample and standard mixture was performed with multiple reaction monitoring (MRM) analysis using MS/MS without chromatographic purification. To each of the standard SAHAs or SAHA-lipid conjugates in liposomal suspension (0.65 ml) was added ethanol (0.25 ml) and 12 M HCl (0.15 ml). After incubating for one hour at 50 °C, the mixture was neutralized to pH 7 with 6 M NaOH at 0 °C and extracted twice with ethyl acetate. The organic layer was collected, washed with brine and concentrated. The resulting extract was dissolved in methanol (0.20 ml) to afford a standard or sample solution of SAHA.

For MS/MS analysis, SAHA was analyzed by ESI-LC-MS/MS on a triple-quadrupole mass spectrometer (API-3000; Applied Biosystems). The instrument was operated with a turbo ion spray interface in positive ion mode. Analyst 1.4.1 software (Applied Biosystems) was used to control equipment, data acquisition, and the MRM experiment. The parameters in the method are as follows: dwell time, 1000 ms; MRM transition, *m/z* 265 in Q1 and *m/z* 232 in Q3; declustering potential, 45 V; collision energy, 25 V; source temperature, 350 °C and ion spray voltage, 5000 V. The amount of SAHA in the mixture was determined from the calibration curves constructed from four standards ranging from 0.05 to 1.00 μg/ml of SAHA.

Cell Culture Human cervix epithelial adenocarcinoma HeLa cells were obtained from the European Collection of Cell Culture (Wiltshire, U.K.). Murine colon carcinoma Colon 26 cells were obtained from the Cell Resource Center for Biomedical Research, Tohoku University (Miyagi, Japan). Colon 26 cells were grown in RPMI-1640 medium (Invitrogen, Carlsbad, CA, U.S.A.) and HeLa cells in Eagle's Minimum Essential Medium (Invitrogen), supplemented with 10% heat-inactivated fetal bovine serum (FBS, Invitrogen) and kanamycin (100 μg/ml) at 37 °C in a 5% CO_2 humidified atmosphere.

Antiproliferative Activity The cells were seeded in 96-well plates 24 h prior to transfection. Cells at 30% confluences in the well were treated with various concentrations of HDACI-lipid conjugates or liposomal HDACI-lipid conjugates for 48 h. Cell viability (%) was measured by WST-8 assay (Dojindo Laboratories, Kumamoto, Japan) as previously reported.[18]

Western Blot Analysis Western blot analysis for acetylated histone H3 and β-actin protein was performed as previously reported.[19] Briefly, Colon 26 cells were seeded in a 35-mm culture dish and incubated overnight. The cells at 30% confluency were treated with liposomal HDACI-lipid conjugates (10 μM as a concentration of HDACI-lipid) or liposomes (L or L-DSPE-PEG) and then incubated for 24 h. The cells were suspended in lysis buffer (1% Triton-X 100 in phosphate-buffered saline pH 7.4 (PBS)), and then Western blotting was performed as previously reported.[19] Acetylated histone H3 was identified using rabbit anti-acetyl histone H3 antibody (Sigma Chemical Co., St. Louis, MO, U.S.A.) and goat anti-rabbit immunoglobulin G (IgG) peroxidase conjugate (Santa Cruz Biotechnology, Santa Cruz, CA, U.S.A.) as the secondary antibody. The blots of β-actin protein were probed with a mouse anti β-actin IgG peroxidase conjugate (β-actin (C4) HRP; Santa Cruz Biotechnology).

Caspase 3/7 Activities Colon 26 cells were seeded in a 35-mm culture dish and incubated overnight. The cells at 30% confluences in the well were treated with liposomal HDACI-lipid conjugates for 24 h. To measure caspase 3/7 activity, a homogenous assay (Caspase-Glo™ 3/7 assay; Promega, Madison, WI, U.S.A.) was performed as previously reported.[18]

Statistical Analysis Significant differences in the mean values were evaluated by Student's unpaired *t*-test. A *p* value of 0.05 or less was considered significant.

Results and Discussion

SAHA is orally administrated because of its hydrophobic property, and is easily metabolized in the liver[12,13]; therefore, we decided to incorporate a potent hydroxamic acid, HDACI, SAHA or K-182,[15] into the liposomal membrane to allow their intravenous administration and increase their acculturation in the tumor by the EPR effect. Liposomal HDACI formulation warrants *in vivo* experiment; however, the amount of hydrophobic drugs incorporated into liposomal membrane was limited. Therefore, we decided to synthesize HDACI-

Table 1. Formulation, Particle Size and ζ-Potential of Liposomal HDACI-Lipid Conjugates

Liposome	Formulation (mol% ratio)	Size (nm)	Polydispersity index	ζ-Potential (mV)
L	DSPC/Chol (55 : 45)	138.9	0.28	1.9±1.1
L-CM-SAHA	DSPC/CM-SAHA (55 : 45)	981.5	0.35	18.5±1.2
L-CM-K-182	DSPC/CM-K-182 (55 : 45)	311.1	0.16	26.4±1.6
L-CCS-K-182	DSPC/CCS-K-182 (55 : 45)	153.8	0.20	36.3±0.5
L-DSPE-PEG	DSPC/Chol/DSPE-PEG_{2000} (52 : 43 : 5)	86.6	0.26	−63.4±2.9
L-DSPE-PEG-SAHA	DSPC/Chol/DSPE-PEG_{2000}-SAHA (52 : 43 : 5)	110.5	0.13	−43.6±1.6
L-OL-PEG-SAHA	DSPC/Chol/OL-PEG_{2000}-SAHA (52 : 43 : 5)	131.2	0.16	−31.6±2.9
L-DSPE-PEG-K-182	DSPC/Chol/DSPE-PEG_{2000}-K-182 (52 : 43 : 5)	90.2	0.23	−29.8±0.4

L: Liposome.

lipid conjugates to increase the amount of HDACI incorporated into the liposomal membrane.

Accordingly, we designed lipid conjugates of SAHA and K-182, in which their hydroxyl (OH) group is tethered to an aliphatic fatty acid or a cholesteryl group *via* linkers connected with biodegradable ester or disulfide carbonate bonds (Fig. 1). The disulfide carbonate linker in a cholesteryl K-182, CCS-K-182, and a PEG_{2000}-lipid conjugate of K-182, DSPE-PEG-K-182, is designed to release unmodified K-182 in the reductive cytosolic condition.[15] We synthesized these compounds using the procedures shown in Charts 1 and 2. The cholesteryl group of CM-K-182 and CM-SAHA is linked with succinic diester bonds, formed by coupling cholesteryl succinate to the original HDACIs, as described previously.[15] The PEG_{2000}-lipid conjugates of SAHA, DSPE-PEG-SAHA and OL-PEG-SAHA, were furnished with a reaction between SAHA and commercially available *N*-hydroxysuccinimide (NHS) ester of DSPE-PEG_{2000} or oleyl-PEG_{2000} followed by purification with LH-20 gel filtration column chromatography.

For preparation of liposomal HDACI-lipid conjugates, the formulation of DSPC/Chol (L) or DSPC/Chol/DSPE-PEG_{2000} (L-DSPE-PEG), which was often used for *in vivo* experiments,[20—22] was modified by substitution of a component (Chol in L or DSPE-PEG_{2000} in L-DSPE-PEG) with HDACI-lipid conjugate. For preparation of liposomal HDACI-Chol conjugate, Chol of liposome (L) formulation was substituted with CCS-K182, CM-K182 and CM-SAHA (L-CCS-K-182, L-CM-K-182 and L-CM-SAHA, respectively) (Table 1). For liposomal HDACI-PEG-lipid conjugates, DSPE-PEG_{2000} of L-DSPE-PEG formulation was substituted with OL-PEG-SAHA, DSPE-PEG-SAHA and DSPE-PEG-K-182 (L-OL-PEG-SAHA, L-DSPE-PEG-SAHA and L-DSPE-PEG-K-182, respectively) (Table 1). The liposomal HDACI-PEG-lipid conjugates were about 90—130 nm with narrow size dispersions and negative ζ-potentials, which might be influenced by PEG coating (Table 1). The liposomal HDACI-Chol conjugates, L-CM-K-182 and L-CCS-K-182 were about 150—300 nm, but L-CM-SAHA was large (about 1 μm) (Table 1). Among liposomal HDACI-Chol conjugates, L-CCS-K-182 and L-CM-K-182 had positive charges in ζ-potential, which might be affected by a ternary amine of K-182. When size and ζ-potential measurements were conducted over a period of one month at 4 °C, no physicochemical changes were observed. After gel filtration, we measured the entrapment efficiency of HDACI-lipid conjugate into the liposome. Entrapment efficiency of HADCI-Chol conjugates into liposomes was almost 100%, but that of HDACI-PEG-lipid conjugates was about 60—70% (data not shown), suggesting that the lipid anchor of HDACI-lipid conjugate might affect modification of the surface of liposomes by HDAC-lipid; however, in subsequent experiments, we used unpurified liposomes for uniform lipid concentration among liposomal HDACI-lipids.

To investigate whether liposomal HDACI-lipid conjugates had antitumor effects on tumor cells, we treated HDACI-lipid conjugates or liposomal HDACI-lipid conjugates with HeLa and Colon 26 cells for 48 h (Table 2). In HDACI-lipid conjugates, CCS-K-182, DSPE-PEG-K-182, DSPE-PEG-SAHA and OL-PEG-SAHA showed high cytotoxicity for both cell lines, but CM-K-182 and CM-SAHA only weakly. In liposomal HDACI-lipid conjugates, L-OL-PEG-SAHA strongly exhibited cytotoxicity for Colon 26 and HeLa cells (IC_{50}=1.4, 4.0 μM, respectively), L-DSPE-PEG-SAHA, L-DSPE-PEG-K-182 and L-CCS-K-182 moderately for HeLa cells (IC_{50}=13.3, 9.9, 3.5 μM, respectively), but L-CM-SAHA and

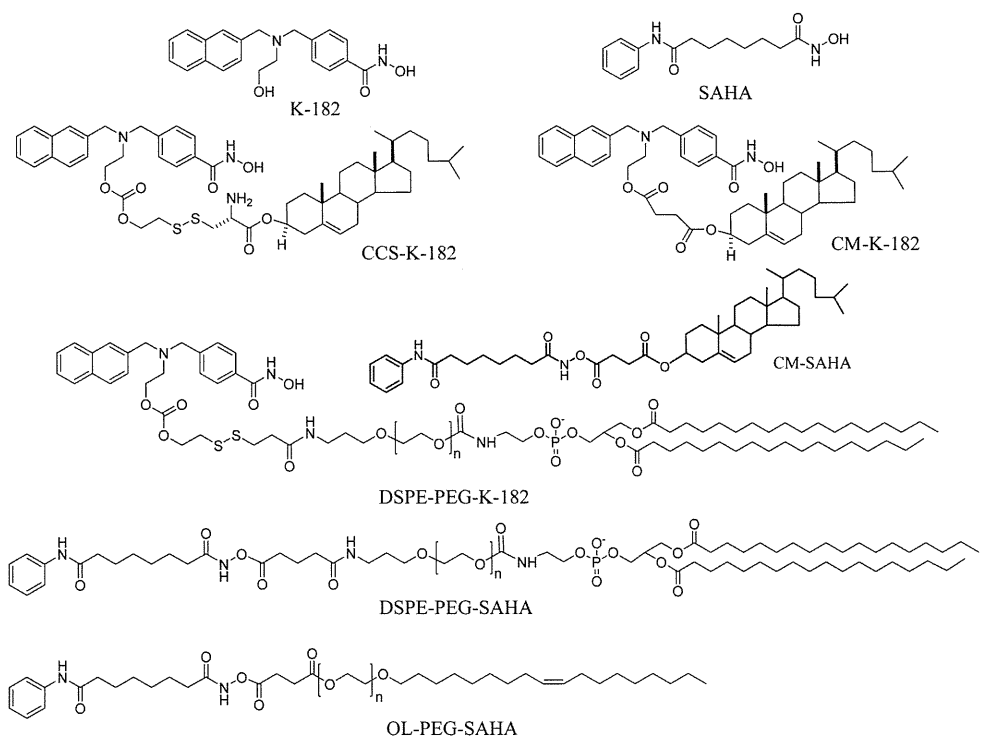

Fig. 1. Chemical Structures of K-182, SAHA, K-182 and SAHA Derivatives

Table 2. IC_{50} Values for HeLa and Colon 26 Cells by HDACI-Lipid Conjugates and Liposomal HDACI-Lipid Conjugates

Drugs	IC_{50} of HDACI or HDACI-lipid conjugates (μM)		IC_{50} of liposomal HDACI-lipid conjugates (μM)	
	HeLa	Colon 26	HeLa	Colon 26
SAHA	1.9	9.5	—	—
K-182	1.0	2.3	—	—
CM-SAHA	19.0	>40.0	18.6	>40.0
CM-K-182	27.4	>40.0	>40.0	>40.0
CCS-K-182	4.6	17.1	3.5	19.4
DSPE-PEG-SAHA	7.6	10.7	13.3	>20.0
OL-PEG-SAHA	1.8	2.4	1.4	4.0
DSPE-PEG-K-182	5.1	7.8	9.9	>20.0

IC_{50} was calculated as a concentration of HDACI or HDACI-lipid conjugate.

L-CM-K-182 did not (Table 2). In particulars, L-OL-PEG-SAHA showed higher cytotoxicity than free SAHA for both cell lines (IC_{50} of free SAHA=1.9, 9.5 μM for HeLa and Colon 26 cells, respectively), suggesting that hydroxamic acid of SAHA might be protected from hydrolysis in the medium by conjugation with lipid. When L and L-DSPE-PEG were treated at the same lipid concentrations with liposomal HDACI-lipid conjugates, they did not show any cytotoxic effects (data not shown). Generally, positively charged liposomes can be easily taken up by the cells *via* electrostatic interaction compared with negatively charged ones, however, cytotoxicities by liposomal HDACI-lipid conjugates were not affected by the physicochemical property and were dependent on structure of HDACI-lipid conjugates.

Histone H3 is one of the core histone proteins in the chromatin of eukaryotic cells. Hyperacetylation of lysine residues, *i.e.* lysine 9, in the N-terminal tails of histone H3 loosens the histone-DNA binding and activates gene transcription. On the other hand, deacetylation of acetylated lysine residues leads to tight histone-DNA binding, which restricts the access of transcriptional factors. Histone acetyltransferases (HATs) and HDACs play a crucial role in this reversible acetylation and deacetylation of histones regulating gene expression. Inhibition of HDACs therefore induces histone hyperacetylation and activates gene transcription.[23] SAHA selectively induces the expression of specific genes such as $p21^{WAF1/CIP1}$ cyclin-dependent kinase inhibitor to effect cell-cycle arrest, resulting in the induction of apoptosis.[24]

We evaluated the acetylation of histone H3 and induction of apoptosis by liposomal HDACI-lipid conjugates (Fig. 2). When liposomal HDACI-lipid conjugates were treated with Colon 26 cells for 24 h, L-CCS-K-182, L-DSPE-PEG-SAHA and L-OL-PEG-SAHA strongly induced the acetylation of histone H3 (Fig. 2A). Furthermore, to examine the effect of histone hyperacetylation on the activity of apoptosis-associated enzymes, we measured caspase 3/7 activity 24 h after treatment with liposomal HDACI-lipid conjugates at 10 μM as a concentration of K-182 or SAHA (Fig. 2B). Among the liposomal HDACI-lipid conjugates, L-OL-PEG-SAHA strongly increased caspase 3/7 activities about 3-fold higher than untreated cells. In L-CCS-K-182, the caspase 3/7 activity was not increased because CCS-K-182 concentration in the medium was under the IC_{50} for Colon 26 cells (19.4 μM). This observation indicated that L-OL-PEG-SAHA could efficiently release SAHA in the cells and inhibit HDAC in the nucleus, resulting in the hyperacetylation of histone H3.

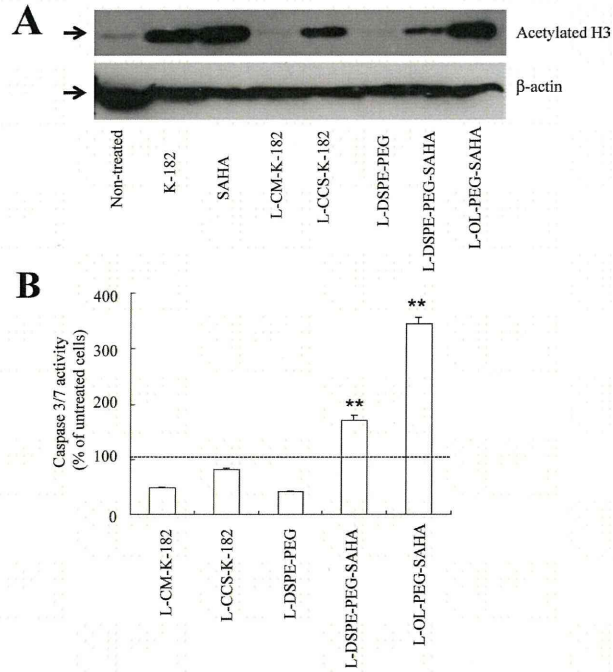

Fig. 2. Acetylation of Core Histone H3 Protein (A) and Induction of Caspase 3/7 Activity (B) by Liposomal HDACI-Lipid Conjugates in Colon 26 Cells

The cells were treated with a medium containing liposomal HDACI-lipid conjugates or free HDACIs. L-DSPE-PEG and L were treated at the same lipid concentration of liposomal HDACI-lipid conjugations. In (A), after 24 h incubation in the medium, cellular proteins were isolated from the cells and resolved on 12.5% SDS-PAGE (10 μg protein in each well), followed by Western blot analysis for acetylated histone H3 protein and β-actin. In (B), after 48 h incubation in the medium, caspase 3/7 activity in Colon 26 cells was measured. Each column shows the mean±S.D. (n=3). ** $p<0.01$, compared with untreated cells.

In antitumor activity, L-CCS-K-182 had antitumor activity *via* acetylation of histone H3, but L-CM-K-182 and L-CM-SAHA did not, suggesting that the disulfide carbonate bond between HDACI and Chol was easily cleavable in cytoplasm, but the ester bond was not. In contrast, L-DSPE-PEG-SAHA, L-DSPE-PEG-K-182 and L-OL-PEG-SAHA had tumor suppressive effects on HeLa cells, indicating that K-182 or SAHA on the PEG-terminal of PEG-lipid *via* a carbamide bond was cleavable in the cells. Among the liposomal HDACI-lipid conjugates, L-OL-PEG-SAHA showed the highest antitumor effect on both HeLa and Colon 26 cells. DSPE-PEG-SAHA was anchored in liposomes *via* two alkyl chains, which could be easily retained liposome compared to OL-PEG-SAHA, which was anchored *via* one alkyl chain. Previously, we synthesized K-182-lipid conjugate, which bound to lipid *via* a carbamide or disulfide linker, into cationic nanoparticles and confirmed that the conjugates were activated by cleavage between K-182 and lipid.[15] Therefore, OL-PEG-SAHA might be efficiently released from L-OL-PEG-SAHA in the cells, and converted to SAHA by the cleavage of carbamide bond. However, it was not clear why L-OL-PEG-SAHA could induce higher cytotoxicity than free SAHA, but OL-PEG-SAHA might be stabilized hydroxamic acid by conjugation with PEG-lipid. We confirmed that oleyl-PEG_{2000} did not show cytotoxicity at the concentra-

tions used in this study (data not shown).

Liposomes take advantage of the EPR effect for increasing their tumor accumulation when they are intravenously injected.[14] Liposomal HDACI-lipid conjugates might improve the pharmacokinetic and pharmacodistribution of the encapsulated drug. Liposomal LAQ824, hydrophilic hydroxamic acid HDAC inhibitor, was shown to be both long-circulating and highly stable *in vivo*.[14] In further study, we need to evaluate whether liposomal HDACI-lipid conjugation has antitumor effects by intravenous injection. Liposomal HDACI-lipid conjugates might have potential as an effective vector in cancer therapy.

In this study, we synthesized HDACI-lipid conjugates and applied liposomal formulations. Liposomal HDACI-lipid conjugates could induce antitumor activity *via* acetylation of histone H3 and activation of caspase 3/7 in HeLa and Colon 26 tumor cells. These findings indicate that liposomal HDACI-lipid conjugates have potential as an effective vector in cancer therapy.

Acknowledgements This project was supported in part by a Grant-in-Aid for Scientific Research (C) from the Ministry of Education, Culture, Sports, Science, and Technology of Japan, KAKENHI (21590131), and by the Open Research Center Project.

References

1) Nightingale K. P., O'Neill L. P., Turner B. M., *Curr. Opin. Genet. Dev.*, **16**, 125—136 (2006).
2) Wade P. A., Pruss D., Wolffe A. P., *Trends Biochem. Sci.*, **22**, 128—132 (1997).
3) Marchion D., Münster P., *Expert Rev. Anticancer Ther.*, **7**, 583—598 (2007).
4) Elaut G., Török G., Vinken M., Laus G., Papeleu P., Tourwe D., Rogiers V., *Drug Metab. Dispos.*, **30**, 1320—1328 (2002).
5) Vanhaecke T., Papeleu P., Elaut G., Rogiers V., *Curr. Med. Chem.*, **11**, 1629—1643 (2004).
6) Marks P., Rifkind R. A., Richon V. M., Breslow R., Miller T., Kelly W. K., *Nat. Rev. Cancer*, **1**, 194—202 (2001).
7) Butler L. M., Agus D. B., Scher H. I., Higgins B., Rose A., Cordon-Cardo C., Thaler H. T., Rifkind R. A., Marks P. A., Richon V. M., *Cancer Res.*, **60**, 5165—5170 (2000).
8) Richon V. M., Webb Y., Merger R., Sheppard T., Jursic B., Ngo L., Civoli F., Breslow R., Rifkind R. A., Marks P. A., *Proc. Natl. Acad. Sci. U.S.A.*, **93**, 5705—5708 (1996).
9) Heymann W. R., *J. Am. Acad. Dermatol.*, **59**, 696—697 (2008).
10) Vansteenkiste J., Van Cutsem E., Dumez H., Chen C., Ricker J. L., Randolph S. S., Schöffski P., *Invest. New Drugs*, **26**, 483—488 (2008).
11) Luu T. H., Morgan R. J., Leong L., Lim D., McNamara M., Portnow J., Frankel P., Smith D. D., Doroshow J. H., Wong C., Aparicio A., Gandara D. R., Somlo G., *Clin. Cancer Res.*, **14**, 7138—7142 (2008).
12) Du L., Musson D. G., Wang A. Q., *Rapid Commun. Mass Spectrom.*, **19**, 1779—1787 (2005).
13) Kelly W. K., Richon V. M., O'Connor O., Curley T., MacGregor-Curtelli B., Tong W., Klang M., Schwartz L., Richardson S., Rosa E., Drobnjak M., Cordon-Cordo C., Chiao J. H., Rifkind R., Marks P. A., Scher H., *Clin. Cancer Res.*, **9**, 3578—3588 (2003).
14) Drummond D. C., Marx C., Guo Z., Scott G., Noble C., Wang D., Pallavicini M., Kirpotin D. B., Benz C. C., *Clin. Cancer Res.*, **11**, 3392—3401 (2005).
15) Ishii Y., Hattori Y., Yamada T., Uesato S., Maitani Y., Nagaoka Y., *Eur. J. Med. Chem.*, **44**, 4603—4610 (2009).
16) Xie H., Braha O., Gu L. Q., Cheley S., Bayley H., *Chem. Biol.*, **12**, 109—120 (2005).
17) Gediya L. K., Chopra P., Purushottamachar P., Maheshwari N., Njar V. C., *J. Med. Chem.*, **48**, 5047—5051 (2005).
18) Hattori Y., Hakoshima M., Koga K., Maitani Y., *Int. J. Oncol.*, **36**, 1039—1046 (2010).
19) Hattori Y., Fukushima M., Maitani Y., *Int. J. Oncol.*, **30**, 1427—1439 (2007).
20) Parr M. J., Masin D., Cullis P. R., Bally M. B., *J. Pharmacol. Exp. Ther.*, **280**, 1319—1327 (1997).
21) Hattori Y., Shi L., Ding W., Koga K., Kawano K., Hakoshima M., Maitani Y., *J. Controlled Release*, **136**, 30—37 (2009).
22) Hong R. L., Huang C. J., Tseng Y. L., Pang V. F., Chen S. T., Liu J. J., Chang F. H., *Clin. Cancer Res.*, **5**, 3645—3652 (1999).
23) Strahl B. D., Allis C. D., *Nature* (London), **403**, 41—45 (2000).
24) Richon V. M., Sandhoff T. W., Rifkind R. A., Marks P. A., *Proc. Natl. Acad. Sci. U.S.A.*, **97**, 10014—10019 (2000).

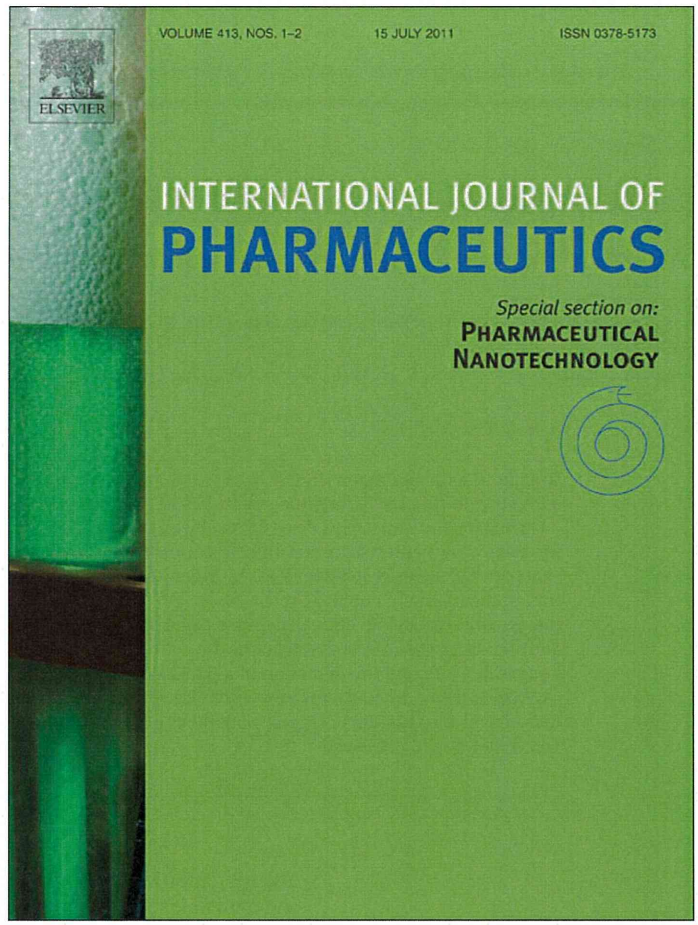

International Journal of Pharmaceutics 413 (2011) 271–278

Contents lists available at ScienceDirect

International Journal of Pharmaceutics

journal homepage: www.elsevier.com/locate/ijpharm

Pharmaceutical Nanotechnology

Organic nanotubes for drug loading and cellular delivery

Ai Wakasugi[a], Masumi Asakawa[b], Masaki Kogiso[b], Toshimi Shimizu[b], Mamiko Sato[c], Yoshie Maitani[a,*]

[a] Institute of Medicinal Chemistry, Hoshi University, Tokyo, Japan
[b] Nanotube Research Center (NTRC), National Institute of Advanced Industrial Science and Technology (AIST), Tsukuba, Japan
[c] Laboratory of Electron Microscopy, Japan Women's University, Tokyo, Japan

ARTICLE INFO

Article history:
Received 11 March 2011
Accepted 15 April 2011
Available online 21 April 2011

Keywords:
Organic nanotube
Cellular uptake
Drug loading
Folate modification
Drug release
Doxorubicin

ABSTRACT

Organic nanotubes made of synthetic amphiphilic molecules are novel materials that form by self-assembly. In this study, organic nanotubes with a carboxyl group (ONTs) at the surface were used as a carrier for the anticancer drug doxorubicin, which has a weak amine group. The IC_{50} values of ONT for cells were higher than that of conventional liposomes, suggesting that ONTs are safe. The results showed that the drug loading of ONTs was susceptible to the effect of ionic strength and H^+ concentration in the medium, and drug release from ONTs was promoted at lower pH, which is favorable for the release of drugs in the endosome after cellular uptake. ONTs loaded with the drug were internalized, and the drug was released quickly in the cells, as demonstrated on transmission electron microscopy images of ONTs and the detection of a 0.05% dose of ONT chelating gadolinium in the cells. Moreover, ONT could be modified chemically with folate by simply mixing with a folate-conjugate lipid. Therefore, these novel, biodegradable organic nanotubes have the potential to be used as drug carriers for controlled and targeting drug delivery.

1. Introduction

Particle dosage forms have been receiving much attention as drug delivery systems (DDS), because of features such as controlled release, absorption improvement, and drug targeting. A variety of drug carriers, such as liposomes and polymer micelles, have been investigated (Bangham et al., 1965; Yokoyama et al., 1991), and their efficiency depending on carriers is reported. Currently, non-spherical carriers have received attention. Nonspereical particles were internalized in HeLa cells (Gratton et al., 2008). In this regard, we focused on organic nanotubes as a novel drug carrier. Organic nanotubes have a cylindrical structure that self-assembles from amphiphilic molecules in aqueous media. Organic nanotubes have an inner diameter of 10–200 nm, an outer diameter of 40–1000 nm, and a length of approximately 2 μm to several hundred μm. Furthermore, these dimensions are controllable by rationalizing the molecular structure of the amphiphilic molecules (John et al., 2001; Kamiya et al., 2005; Shimizu et al., 2005; Kogiso et al., 2007). Organic nanotubes can entrap proteins, nucleic acids, viruses, and metal nanoparticles, which cannot be achieved using cyclodextrin because organic nanotubes have at least a 10-fold larger inner diameter providing much greater space for the encapsulation of passenger molecules than cyclodextrin. Similar to cyclodextrin, organic nanotubes are expected to be applied for use in the medical and food fields (Yang et al., 2004a,b; Yui et al., 2005; Shimizu, 2006, 2008a; Kameta et al., 2005, 2007, 2008).

Organic nanotubes were first discovered to self-assemble from amphiphilic molecules in the pioneering work of Yager and Schoen (1983), Kunitake's (Nakashima et al., 1984), and Hirayama's (Yamada et al., 1984) research groups, among others, using diacetylenic phospholipids and glutamate derivatives. However, applications for these organic nanotubes have not been studied because the efficient mass production of these molecules has never been achieved. Interestingly, after the self-assembly of newly designed molecules in alcoholic solvents, such as ethanol, we found that evaporation of the solvent left tubular material in quantities more than 1000-fold greater than those when using the same volume of water (Shimizu, 2008b; Asakawa et al., 2009). Thus, 100 g of organic nanotubes can be readily produced in a laboratory and 10 kg in a factory. As a result, the stable supply of organic nanotubes has become possible, and the searches for applications in many fields have begun in earnest.

This is the first report to examine potential drug delivery application of the organic nanotubes with a carboxyl group (ONTs) at the surface. In this study, the anticancer drug doxorubicin (DXR) was selected for loading into ONTs. DXR has a weak amine group and has been reported to be entrapped into many particle carriers such as polymer micelles, liposomes, and carbon nanotubes (Yokoyama et al., 1991; Cabanes et al., 1998; Liu et al., 2007). Information on ONT loading with DXR will help to compare these

* Corresponding author. Tel.: +81 3 5498 5048; fax: +81 3 5498 5048.
E-mail address: yoshie@hoshi.ac.jp (Y. Maitani).

0378-5173/$ – see front matter © 2011 Elsevier B.V. All rights reserved.
doi:10.1016/j.ijpharm.2011.04.038

different carriers. Loading of DXR into ONT and the release of DXR from ONT were controlled by varying the pH and ionic strength in the medium. ONT loaded with the drug was taken up by non-phagocytic mouse colon adenocarcinoma 26 cell line (C26) cells, and the drug was released quickly in the cells. Furthermore, ONTs were functionalized by associating with a folate-conjugated lipid non-covalently.

2. Materials and methods

2.1. Materials

ONTs were prepared at the Nanotube Research Center (NTRC), National Institute of Advanced Industrial Science and Technology (AIST) (Tsukuba, Japan). ONT1 and ONT2 are easily formed by the evaporating methanol solutions of compounds **1** and **2**, respectively (Fig. 1) (Kogiso et al., 2010a). Gd^{3+}-complexed ONT1 (Gd-ONT1), which contained 12.6 wt% of gadolinium(III) ions, was also formed from $GdCl_3$ and compound **1** as described previously (Kogiso et al., 2010b). Methoxy-poly(ethyleneglycol)-distearylphosphatidylethanolamine (PEG_{2000}-DSPE, PEG mean molecular weight, 2000) and amino-PEG_{2000}-DSPE were purchased from NOF Corporation (Tokyo, Japan). DXR hydrochloride was purchased from Wako Pure Chemical Industries Ltd. (Osaka, Japan). Folate-PEG_{2000}-DSPE conjugate of folic acid (F-PEG-DSPE) was synthesized from amino-PEG-DSPE as reported previously (Gabizon et al., 1999). RPMI-1640 medium, folate-deficient RPMI-1640 medium, and fetal bovine serum (FBS) were obtained from Invitrogen Corp. (Carlsbad, CA, USA). Other reagents used in this study were of reagent grade.

2.2. Cell culture

Mouse colon adenocarcinoma 26 cell line (C26) and a human nasopharyngeal cancer cell line (KB) were obtained from the Cell Resource Center for Biomedical Research, Tohoku University (Miyagi, Japan). The cells were cultured in RPMI-1640 medium or folate-deficient RPMI-1640 medium containing 10% heat-inactivated FBS and 100 μg/mL kanamycin sulfate in a humidified atmosphere containing 5% CO_2 at 37 °C.

2.3. Preparation of ONTs loaded with DXR

2.3.1. DXR loading into ONTs

To prepare ONTs loaded with DXR (DXR/ONT), ground ONT (~2 mg, a length of approximately 2 μm) and DXR aqueous solutions (1 mg/mL, 100 μL) were mixed, then vortexed for 10 min, and sonicated. Then, 900 μL of deionized and filtered water (water), PBS (pH 7.4), or McIlvaine buffer (pH 4, 6, or 8) was added to the mixture of DXR and ONTs. To measure the entrapment efficiency of DXR into ONTs, the mixing weight ratio of ONTs and DXR and the medium were changed. After mixing, DXR and ONT in the medium were centrifuged (20,400 × *g*, 20 °C, 30 min), the precipitate was washed with water (DXR/ONT), and the DXR concentration in the supernatant was analyzed by HPLC (Barth and Conner, 1977). The HPLC system was composed of an LC-20AT pump (Shimadzu Co.), SIL-20A autoinjector (Shimadzu Co.), RF-10AXL fluorescence detector (Shimadzu Co.), and YMC-PACK Pro C18 RS, 150 mm × 4.6 mm i.d. column (YMC Co. Ltd., Kyoto, Japan). The isocratic mobile phase was 3:7 (v/v) acetonitrile:ammonium formate, adjusted to pH 4.0 with formic acid, running at a flow rate of 1.0 mL/min. Daunorubicin was used as the internal standard (i.s.). Daunorubicin and DXR were detected by excitation and emission wavelengths of 485 and 535 nm, respectively. Then, the loading amount and loading efficiency were calculated using the following equations:

$$\text{Loading amount}\,(\mu g/mg) = \frac{\text{added DXR}\,(\mu g) - \text{remained DXR in supernatant}\,(\mu g)}{\text{ONT amount}\,(\mu g)}$$

$$\text{Loading efficiency}\,(\%) = \frac{\text{added DXR}\,(\mu g) - \text{remained DXR in supernatant}\,(\mu g)}{\text{added DXR}\,(\mu g)} \times 100$$

2.3.2. DXR/folate-modified ONT1

DXR/folate-modified ONT1 (DXR/F-ONT1) was prepared by mixing DXR/ONT1 at a weight ratio of 1:20 with PBS at pH 7.4. then, a 0.25, 0.5, or 2.5 mol% of F-PEG-DSPE solution was added to 2 mg/mL DXR/ONT1 suspended in water, which was then incubated overnight and centrifuged at 20,400 × *g* for 30 min at 20 °C to separate DXR/F-ONT1 and free F-PEG.-DSPE. To confirm folate modification, the DXR/F-ONT1 suspension was irradiated with UV light at 253.7 nm for 1 h. After centrifugation at 20,400 × *g* for 30 min, degraded folate (pterine-6-carboxylic acid) in the supernatant was detected using a fluorescence spectrophotometer (Hitachi High-Tech, Tokyo, Japan) with an excitation wavelength of 350 nm and emission wavelength at 350–600 nm. DXR/PEG-modified ONT1 (DXR/PEG-ONT1) was also prepared by the same method using PEG-DSPE instead of F-PEG-DSPE.

2.4. Drug release from ONT1

The release of DXR from DXR/ONT1 in a dialysis tube was measured using seamless cellulose tube membranes (Viskase Sales Corp., IL, USA) with a molecular weight cutoff of 100,000. The initial concentration of DXR was 100 μg/mL. The sample volume in the dialysis tube was 1 mL and the sink volume was 100 mL of PBS at pH 7.4 or 5.5 with the same ionic strength, adjusted by the addition of sodium chloride or water at 37 °C (Johnston et al., 2006). The DXR concentration was analyzed using HPLC as described in Section 2.3.1. The release of DXR from ONT1 at pH 7.4 or pH 5.5 was corrected by characterizing the release of free DXR as adsorption of DXR using the dialysis membrane.

2.5. Cytotoxicity study

C26 or KB cells were prepared by plating 1×10^4 cells in a 96-well culture Plate 1 day before the experiment. Cells were then incubated with the ONTs, DXR, DXR/ONT1 and DXR/F-ONT1 diluted in RPMI-1640 medium or folate-deficient RPMI-1640 medium containing 10% heat-inactivated FBS for 48 h at 37 °C. Cytotoxicity was determined using a WST-8 assay (Dojindo Laboratories, Kumamoto, Japan). The number of viable cells was then determined by absorbance measured at 450 nm using an automated plate reader (BioRad, Hercules, CA, USA).

2.6. Flow cytometry analysis

ONT1 was labeled with 1,1′-dioctadecyl-3,3,3′,3′-perchlorate (DiI) to evaluate cellular uptake. An ethanolic solution of DiI (0.1 mol% of ONT1) was added to the ONT suspension in PBS (pH 7.4), which was incubated for 3 days and then centrifuged 20,400 × *g* at 20 °C for 30 min (DiI-labeled ONT1). The resulting precipitate was resuspended in culture medium. C26 and KB cells were prepared by plating 1×10^6 cells/well in a 6-well culture Plate 1 day before assaying. Cells were incubated with DiI-labeled ONT1 or DXR/F-ONT1 at less than 200 μg/mL ONT1 in RPMI-1640 medium or folate-deficient RPMI-1640 medium, respectively, containing

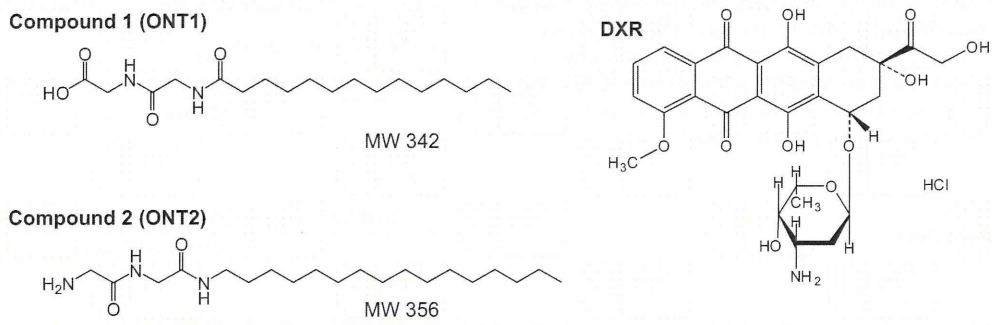

Fig. 1. Chemical structures of compound **1**, compound **2**, and doxorubicin (DXR). Compound **1** forms organic nanotube 1 (ONT1) and compound **2** forms ONT2. Compound **1** consists of glycylglycine and myristic acid, and compound **2** consists of glycylglycine and hexadecylamine.

10% heat-inactivated FBS for 1 or 24 h at 37 °C. After incubation, the cells were washed with cold PBS two times, detached with 0.05% trypsin or EDTA, respectively, and then suspended in PBS containing 0.1% bovine serum albumin and 1 mM EDTA. The suspended cells were directly introduced into a FACSCalibur flow cytometer (Becton Dickinson, San Jose, CA, USA) equipped with a 488 nm argon ion laser. Data for 10,000 fluorescent events were obtained by recording forward scatter and side scatter with 530/30 nm fluorescence. The autofluorescence of cells was taken as a control.

2.7. Confocal microscopy

After incubation with DiI-labeled ONT1 for 1 or 24 h as described above, the medium was removed, and the cells were washed three times with PBS and fixed with 10% formaldehyde in PBS at 37 °C for 20 min. Then, the cells were coated with Aqua Poly/Mount (Polyscience, Warrington, PA, USA) to prevent fading and covered with coverslips. The fixed cells were observed using a LSM5 EXCITER confocal laser scanning microscope (Carl Zeiss, Thornwood, NY, USA). For DiI, maximal excitation was performed using a 543-nm internal He-Neon laser, and fluorescence emission at 565 nm was observed with a LP560. Nucleic acids were stained using SYTOX Green (Invitrogen Corp. Carlsbad, CA, USA), and images were obtained using excitation with an argon laser at 488 nm and fluorescence emission at 523 nm with a filter, BP505-530.

2.8. Determination of cellar uptake of a Gd-ONT1

C26 cells were prepared as a confluent layer in a 10-cm diameter culture plate for the assay. Cells were incubated with 200 μg/mL of Gd-ONT1 in 5 mL of RPMI-1640 medium containing 10% heat-inactivated FBS for 3 h at 37 °C. After incubation, the cells were washed two times with PBS at pH 7.4 and lysed with 1 mL of PBS containing 0.2% Triton X-100 per dish. Associated amounts of Gd in the lysed cells were measured using an inductively coupled plasma (ICP) assay using an SPS7800 apparatus (SII NanoTechnology Inc., Tokyo, Japan). The amount of cellular uptake was calculated using the following equation:

$$\text{Dose}(\%) = \frac{\text{cellular uptake of Gd-ONT1 (mg)}}{\text{applied Gd-ONT1 (mg)}} \times 100$$

2.9. TEM observation

C26 or KB cells were prepared at 70% confluency on Aclar film (NISSIN EM, Tokyo) 1 day before the experiment. Cells were then incubated with 10 μg/mL ONT1 or F-ONT1 diluted in RPMI-1640 medium or folate-deficient RPMI-1640 medium, respectively containing 10% heat-inactivated FBS for 1 and 24 h at 37 °C. After incubation, the cells were washed three times with PBS at pH 7.4 and fixed with 2% glutaraldehyde in PBS (pH 7.4) for 2 h at 4 °C. After washing, the cells were postfixed with 1% osmium tetroxide in PBS (pH 7.4) for 2 h at 4 °C, and washed again with the same buffer. The fixed specimens were stained with 1% uranyl acetate for 1 h at 4 °C, dehydrated with a graded ethanol series, and embedded in the Quetol 812 mixture (NISSIN EM, Tokyo). Ultrathin sections were stained with 4% uranyl acetate and 0.4% lead citrate and observed using a JEM-1200EXS (JEOL Ltd., Tokyo) at 80 kV.

2.10. Statistical analysis

The results are expressed as the mean ± S.D. Statistical comparisons were performed using Student's *t*-test. *P* values less than 0.05 were considered significant.

3. Results

3.1. Characterization of ONTs

ONT1 had an inner diameter of 30–40 nm, an outer diameter of 70–90 nm, and a gel-to-liquid crystalline phase transition temperature of approximately 60 °C. ONT2 had similar characteristics to ONT1. The cytotoxicity of ONT1 in C26 cells and KB cells was examined. For both cell lines, death was induced at a concentration above 200 μg/mL for ONT1, as shown in Fig. 2. The IC_{50} values for KB cells and C26 cells were 200 and 171.1 μg/mL, respectively. These values are higher than that for conventional liposomes (Kajiwara et al., 2007), suggesting that ONT1 is safe to use.

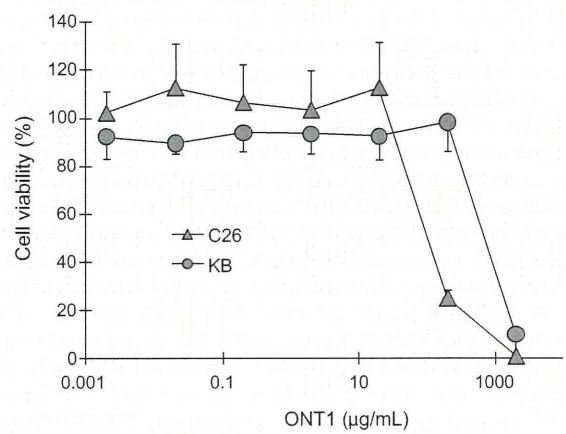

Fig. 2. Cytotoxicity of ONT1 in C26 cells or KB cells treated for 48 h. Each value represents mean ± S.D. ($n = 4$).

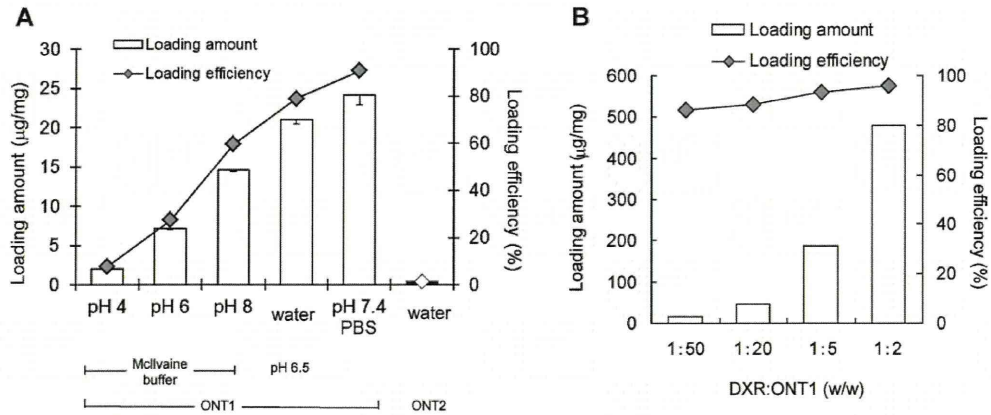

Fig. 3. Loading amount and loading efficiency of DXR into ONTs at a DXR/ONT weight ratio of ~0.05 in various buffers (A) and various ratios of DXR:ONT1 (w/w) in PBS at pH 7.4 (B). Each value represents mean ± S.D. ($n = 3$).

3.2. DXR loading and release from ONT1

First, to examine the effect of pH on the loading of DXR into ONTs, McIlvaine buffer at pH 4, 6, or 8 (ionic strength, 1.0) was used as a medium. DXR loading efficiency into ONT1 at a weight ratio of DXR/ONT of 1:20 increased from 2 to 15 μg DXR/mgONT1 when the pH of the medium was increased from pH 4 to 8 (Fig. 3A). The preparation of DXR/ONT1 using McIlvaine buffer indicated that DXR loading efficiency increased depending on the increasing pH of the medium. Next, to examine the effect of ionic strength on loading efficiency; water and pH 7.4 physiological buffer (PBS, ionic strength, 0.2) were used as the media. Loading efficiency with water at pH 6.5 was substantially higher than that with McIlvaine buffer at the corresponding pH. The loading efficiency with PBS at pH 7.4 was the highest (90%) among those media tested (Fig. 3A). This finding indicated that lower ionic strength and higher pH increased DXR loading. To examine the interaction of the carboxyl group of ONT1 with DXR, ONT2 with an amino group was used. In contrast, DXR in water was hardly loaded into ONT2.

Next, the effect of the weight ratio of DXR and ONT1 on DXR loading was examined (Fig. 3B). As the DXR:ONT1 ratio increased, DXR loading increased to 480 μg/mg. A weight ratio of DXR:ONT1 = 1:20 in PBS at pH 7.4 was selected as the drug loading condition in the following experiment because of the adequate loading efficiency (88%), the amount loaded (44.2 μg/mg), and the easy of handling. The DXR/ONT1 was confirmed to retain nanotube structure using microscope because non-spherical size was not able to measure using dynamic light scattering method.

DXR release from the DXR/ONT1 prepared as described above was evaluated for 72 h in water or PBS at pH 7.4 and 5.5. DXR was not released from DXR/ONT1 in water (data not shown). The release of DXR from ONT1 in PBS at pH 5.5 was promoted compared with that at pH 7.4 (Fig. 4).

3.3. Cellular uptake of ONT1

To evaluate the cellular uptake of ONT1 itself, DiI-labeled ONT1 was incubated with C26 cells for 1 and 24 h. Intracellular fluorescence of DiI-labeled ONT1 increased significantly in a time-dependent manner, as detected by flow cytometry (Fig. 5A). In addition, the cellular uptake of DXR/ONT1 was evaluated by cytotoxicity at a concentration of ONT1 below its IC_{50}. DXR/ONT1 exhibited cell death and apoptosis using a 48 h incubation period, similar to free DXR (Fig. 5B). The IC_{50} between DXR and DXR/ONT1 was not significantly different. Separately, it was confirmed that drug release from DXR/ONT1 in the culture medium was less than 20% (date not shown).

C26 cells incubated with DiI-labeled ONT1, as shown in Fig. 5A, were also observed using confocal microscopy. Red fluorescence of DiI-labeled ONT1 in the cytoplasm was observed with an increasing incubation time for 1–24 h (Fig. 6A and B). Furthermore, it revealed that ONT1 had very high affinity to the cells because a lot of ONT1 was observed on the cellular surface when incubated for 24 h (Fig. 6C).

Because there is the possibility that DXR released from ONT1 could penetrated into cells, the cellular uptake of Gd-ONT1 was examined. Unlike DXR, conjugated Gd was not released from Gd-ONT1, and free Gd ions cannot penetrate into the cells. Gd concentration in the cell lysis fraction after a 3-h incubation of the Gd-ONT1 with C26 cells was determined. The 0.05% dose of Gd was detected in the cells. Moreover, it was confirmed by TEM that ONT1 and F-ONT1 were present in C26 cells (Fig. 7) and KB cells (data not shown), respectively. As shown in Fig. 7B and C, ONT1 was observed in the cytoplasm near the cell membrane after a 24-h incubation, compared with control, untreated C26 cells (Fig. 7A). From these, the finding indicated that ONT1 was taken up to the cells.

3.4. ONT1 functionalized with folate

3.4.1. Confirmation of folate modification

To functionalize ONT1 for cellular uptake mediated by folate receptors (FR), folate-modified ONT1 loaded with DXR (DXR/F-ONT1) and PEGylated ONT1 loaded with DXR (DXR/PEG-

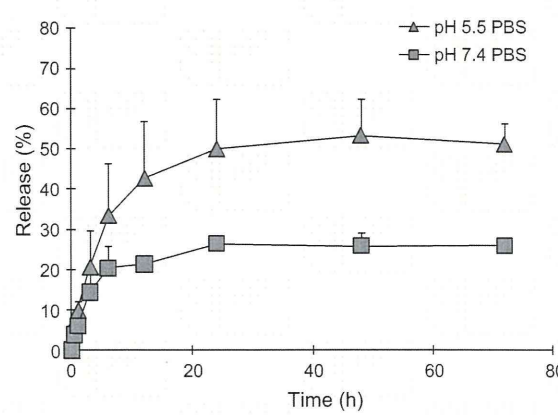

Fig. 4. DXR release from DXR/ONT1 in PBS at pH 5.5 and pH 7.4. Each value represents mean ± S.D. ($n = 3$).

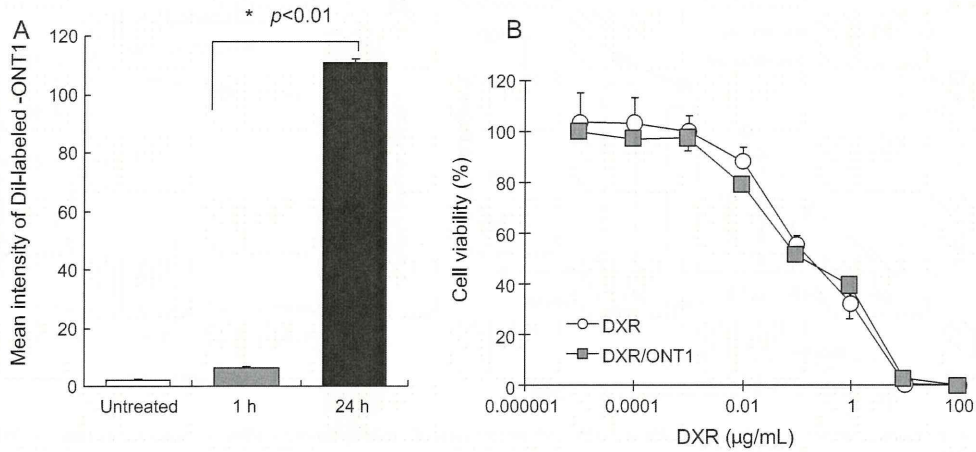

Fig. 5. Evaluation of cellular uptake of ONT1. Cellular uptake of DiI-labeled ONT1 into C26 cells incubated for 1 or 24 h assessed by flow cytometry analysis ($n=3$) (A). Cytotoxicity of free DXR and DXR/ONT1 in C26 cells incubated for 48 h ($n=4$) (B). Each value represents mean ± S.D.

ONT1) as a control were prepared. The folate modification was confirmed using fluorescence detection of pterine-6-carboxylic acid, which is a degradation product of folate after UV irradiation (Akhtar et al., 1999; Hirakawa et al., 2003). As a result of UV irradiation, the fluorescence intensity of DXR/F-ONT1 at 273.5 nm increased depending on the folate modification of ONT1 while no fluorescence of DXR/PEG-ONT1 was detected (Fig. S1). This finding indicated that ONT1 was modified by folate, depending on addition amount of F-PEG-DSPE.

3.4.2. Cellular uptake of F-ONT1

The cellular uptake of DXR/F-ONT1 was investigated by incubation with FR overexpressed in KB cells. DXR/F-ONT1 was modified with various F-PEG-DSPE concentrations (0.25, 0.5, or 2.5 mol% of ONT1), and cellular uptake of DXR/F-ONT1 was evaluated by flow cytometry after 3 h exposure to KB cells. Using a competition assay with free folic acid, the cellular fluorescence intensity of DXR/F-ONT1 modified with 0.5 or 2.5 mol% folate decreased significantly whereas that of DXR/PEG-ONT1 modified with 2.5 mol% PEG-DSPE was not (Fig. 8A). To assess the cellular uptake, the cytotoxicity of DXR/ONT1 modified with 0.25 mol% folate to KB cells was evaluated. The IC_{50} values of DXR/F-ONT1 (0.074 μM) were similar to that of DXR/ONT1 (0.043 μM) and slightly higher than that of free DXR (0.028 μM) (Fig. 8B). This finding suggested that cellular uptake of DXR/F-ONT1 and DXR/ONT1 was similarly fast.

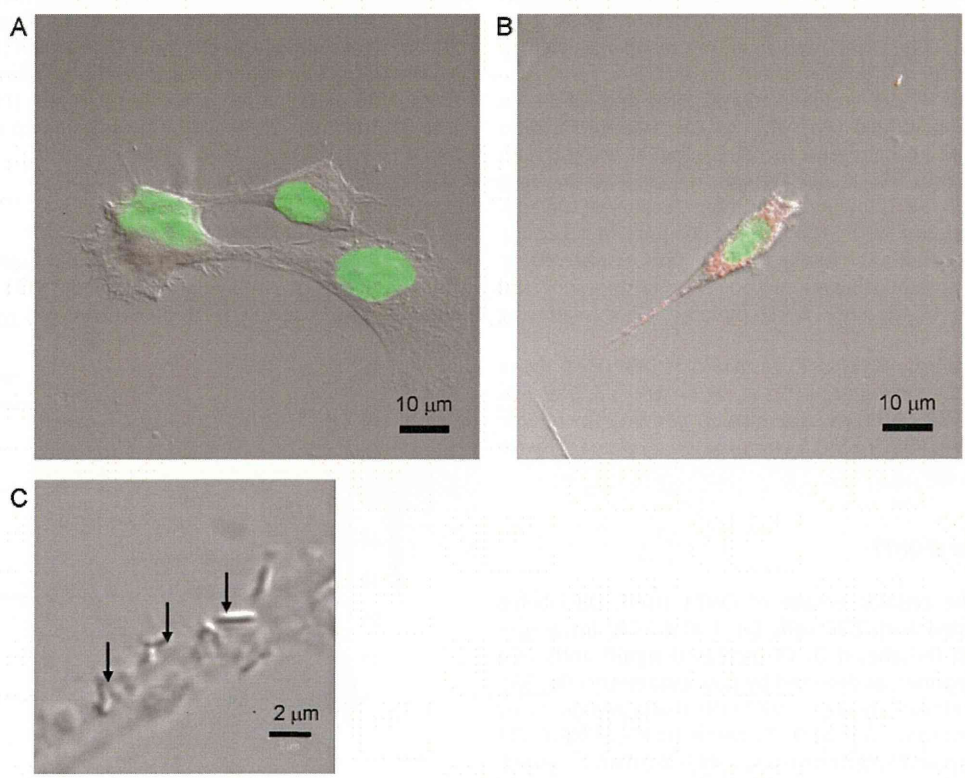

Fig. 6. Cellular uptake of DiI-labeled ONT1 into C26 cells incubated for 1 h (A) or 24 h (B). Red fluorescence indicates DiI and green is a nucleus stained by SYTOX Green. Many ONT1s (arrowhead) were observed at the surface of C26 cells incubated with DiI-labeled ONT1 for 24 h (C).

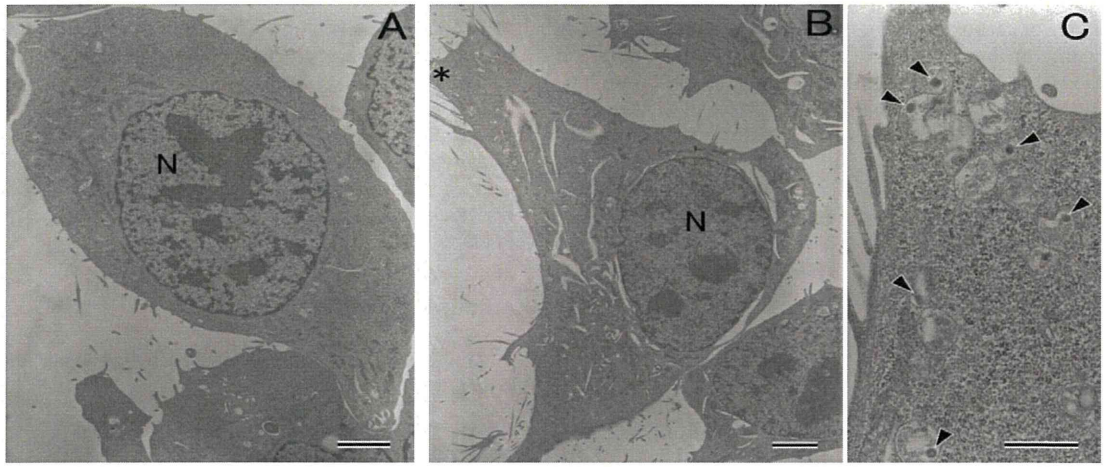

Fig. 7. Transmission electron micrographs showing untreated C26 cells (A) and C26 cells incubated with ONT1 for 24 h (B) and a high magnification image of the surrounding cell (indicated by an asterisk in B) (C). N: nucleus; arrowhead: ONT1, bars = 2 μm (A and B) and 500 nm (C).

4. Discussion

This study showed that at higher pH and a lower ionic strength of the medium, high loading efficiency of DXR into ONT1 and low release of DXR from ONT1 were obtained where the carboxyl group of ONT1 was highly dissociated. Cellular uptake of the DiI-labeled ONT1 into C26 cells was observed by flow cytometry analysis and confocal microscopy. It was also confirmed that Gd-ONT1was detected in the cells and many ONT1s were observed in the endosomes by TEM.

In order to apply ONTs as a drug carrier, their cytotoxicity is of key importance. The cytotoxicity of ONTs in C26 cells and KB cells (IC_{50} 200 and 171.1 μg/mL, respectively) was very low compared with a conventional liposome IC_{50} (8.6 μg/mL) (Kajiwara et al., 2007). Furthermore, it is expected that ONT1 is biodegradable because it is made from edible materials. Thus, ONTs have suitable properties for use as drug carriers.

Drug loading ability and cellular uptake of ONTs were examined using DXR as a model drug because it exhibits autofluorescence and apoptosis inducing activity. ONTs have a nanoscale cylindrical structure; therefore, DXR/ONT was prepared by simply mixing ONT powder with DXR solution by capillary phenomenon. When DXR/ONT was prepared in McIlvaine buffer, the amount of DXR loaded was pH dependent. Higher drug loading efficiency was obtained in PBS at pH 7.4 and lower ionic strength. This result indicated that drug loading into ONT1 was susceptible to the effect of ionic strength and H^+ concentration. The functional group is exposed on the ONT surface, which was supported both by FT-IR spectrum of ONT and by the adsorption of surface-modified gold nanoparticles onto ONT (Kogiso et al., 2010a). ONT1 with a carboxyl group and ONT2 with amino group on their surfaces induced higher and lower levels of DXR loading, respectively. It was supposed that the carboxyl group of ONT1 may interact electrostatically with the amino group of DXR at higher pH where the carboxyl group of ONT1 was highly dissociated. This interaction was decreased in a medium containing electrolytes by electric shielding; therefore, a lower ionic strength of the medium is favorable for preparation of DXR/ONT1.

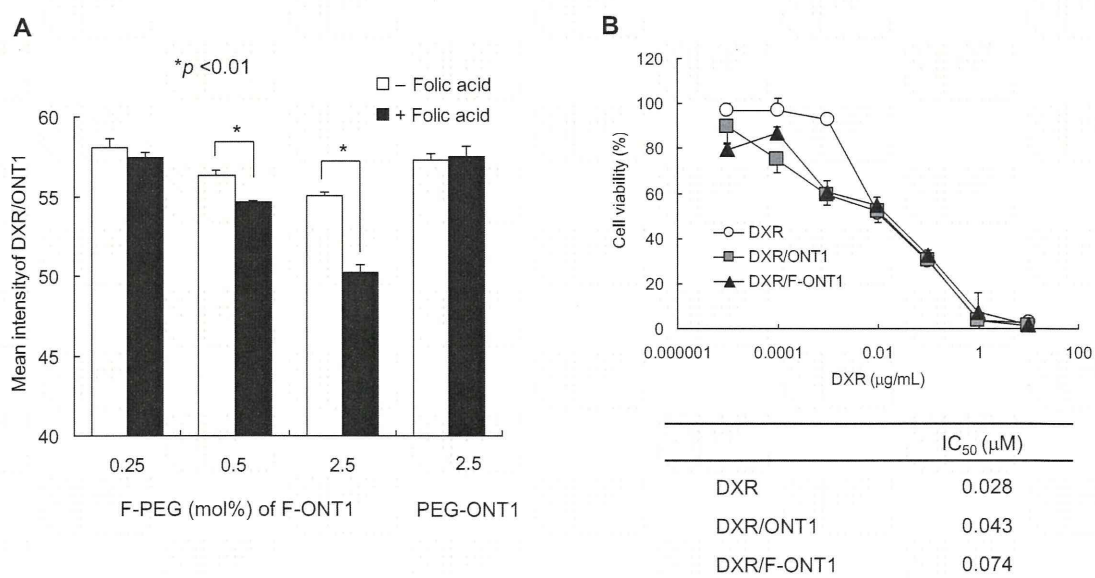

	IC_{50} (μM)
DXR	0.028
DXR/ONT1	0.043
DXR/F-ONT1	0.074

Fig. 8. Evaluation of cellular uptake of ONT1 modified with folate. Cellular uptake of DXR/F-ONT1 and DXR/PEG-ONT1 into KB cells incubated for 3 h was assessed by flow cytometry analysis ($n = 3$) (A). Cytotoxicity of free DXR, DXR/ONT1, and DXR/F-ONT1 modified with 0.25 mol% folate in KB cells incubated for 48 h ($n = 4$) (B). Each value represents mean ± S.D.

The number of carboxylic group per ONT1 is about 2,760,000 estimated using an inner diameter of 50 nm, outer diameter of 80 nm, and length of 2 μm. If the carboxylic group of ONT1 interacts in a 1:1 ratio with an amino group of DXR, 274 μg of DXR will be loaded theoretically into 1 mg of ONT1. In this study, the maximum amount of drug loading was 480 μg DXR/mg ONT1 in a preparation with a 1:2 weight ratio of DXR to ONT1. The DXR loading value was higher compared with that of liposomes (Gokhale et al., 1996). This finding suggested that DXR may insert into each layer.

The release of DXR from ONT1 in PBS at lower pH was higher than that in water. This may be due to a reduction in the electrostatic interaction between DXR and ONT1 because dissociation of the carboxyl group of ONT1 at lower pH and in the presence of electrolytes was reduced. Endosomes are known to function with a typical internal pH value of 5.5 (Wattiaux et al., 2000; Medina-Kauwe et al., 2005), and it was suggested that when DXR/ONT1 was taken up via the endocytotic pathway, the drug should be released quickly from the endosome and will be able to exert its activity. Therefore, drug release from ONT1 at lower pH could be exploited for drug delivery applications for tumor targeting.

Cellular uptake of ONT was evaluated as the cytotoxicity of the loaded DXR activity, which induces apoptosis by intercalation to DNA. The cytotoxic effect of DXR/ONT1 in C26 cells was similar to free DXR. Cellular uptake of DXR/ONT1 and intracellular drug release may occur as rapidly as for free DXR, and/or ONT1 might promote DXR uptake via a specific interaction with the cells. Flow cytometry analysis and confocal microscopy showed time-dependent cellular uptake of the DiI-labeled ONT1 into C26 cells. Gd was detected at a 0.05 dose % in C26 cells incubated with Gd-ONT1 for 24 h. In addition, many ONT1 s were observed in the endosomes by TEM. Although the cellular uptake mechanisms of ONT1 are not clear at present, these results suggest that ONT1 may have high affinity for these cells, and may play an important role in the cellular uptake of the ONT1.

To provide a further possibility for use as a drug carrier, the active targeting ability of ONT1 modified with a target ligand was evaluated. In this study, we focused on cellular uptake via FR. It is known that FR is overexpressed in many human cancer cells, including malignancies of the ovary, mammary gland, kidney, lung, and throat, but is expressed minimally in normal tissues (Kelemen, 2006). Therefore, FR is a good target for selective cancer therapy as a tumor-specific receptor. FRα has a high affinity for folic acid (Kd ~ 0.1 nM; Kamen and Caston, 1986), and its conjugate retains its receptor binding and endocytosis properties in FR positive cancer cells (Leamon and Low, 1991; Anderson et al., 1992; Lu and Low, 2002). We prepared DXR/folate-modified ONT1, DXR/F-ONT1, and evaluated its cellular uptake via FR in KB cells. The cytotoxicity of DXR/F-ONT1 was not significantly different with that of DXR/ONT1. Corresponding to an increase of the modification amount of folate, a competition assay demonstrated that the cellular uptake of DXR/F-ONT1 decreased although the total uptake amount did not increase. It was supposed that cellular pathway through FR for DXR/F-ONT1 uptake and other pathways such as specific for ONT may exist. Therefore, with the addition of free folic acid, increased cellular uptake via FR was not detected, and only inhibition of FR-mediated endocytosis was observed. ONT1 is expected to be an excellent active targeting carrier if folate modification of ONT makes it possible to increase cellular uptake via FR above that for ONT-specific uptake.

5. Conclusions

In this study, we examined the potential of ONT as a drug carrier and demonstrated the following findings; ONT1 can load 480 μg DXR/mg ONT and release the drug rapidly in an acidic environment. DXR/ONT1 was taken up by cells and the drug was released quickly into the cells. Moreover, ONT1 was able to be modified by simply mixing with a folate lipid, which was then taken up through FR. Therefore, these novel, biodegradable organic nanotubes have the potential to be used as drug carriers for controlled and targeted drug delivery. This is the first report on the application of ONTs as drug carriers; however, further in vitro evaluation of interactions with cells must be investigated before this approach can be applied in vivo.

Acknowledgement

This study was supported in part by the Open Research Center Project.

Appendix A. Supplementary data

Supplementary data associated with this article can be found, in the online version, at doi:10.1016/j.ijpharm.2011.04.038.

References

Akhtar, M.J., Khan, M.A., Ahmad, I., 1999. Photodegradation of folic acid in aqueous solution. J. Pharm. Biomed. Anal. 19, 269–275.
Anderson, R.G., Kamen, B.A., Rothberg, K.G., Lacey, S.W., 1992. Potocytosis: sequestration and transport of small molecules by caveolae. Science 255, 410–411.
Asakawa, M., Aoyagi, M., Kameta, N., Kogiso, M., Masuda, M., Minamikawa, H., Shimizu, T., 2009. Development of massive synthesis method of organic nanotube toward practical use. Synthesiology – English Ed. 1, 169–176.
Bangham, A.D., Standish, M.M., Watkins, J.C., 1965. Diffusion of univalent ions across the lamellae of swollen phospholipids. J. Mol. Biol. 13, 238–252.
Barth, H.G., Conner, A.Z., 1977. Determination of doxorubicin hydrochloride in pharmaceutical preparations using high-pressure liquid chromatography. J. Chromatogr. 131, 375–381.
Cabanes, A., Tzemach, D., Goren, D., Horowitz, A.T., Gabizon, A., 1998. Comparative study of the antitumor activity of free doxorubicin and polyethylene glycol-coated liposomal doxorubicin in a mouse lymphoma model. Clin. Cancer Res. 4, 499–505.
Gabizon, A., Horowitz, A.T., Goren, D., Tzemach, D., Mandelbaum-Shavit, F., Qazen, M.M., Zalipsky, S., 1999. Targeting folate receptor with folate linked to extremities of poly(ethylene glycol)-grafted liposomes: in vitro studies. Bioconjug. Chem. 10, 289–298.
Gokhale, P.C., Radhakrishnan, B., Husain, S.R., Abernethy, D.R., Sacher, R., Dritschilo, A., Rahman, A., 1996. An improved method of encapsulation of doxorubicin in liposomes: pharmacological, toxicological and therapeutic evaluation. Br. J. Cancer 74, 43–48.
Gratton, S.E., Ropp, P.A., Pohlhaus, P.D., Luft, J.C., Madden, V.J., Napier, M.E., DeSimone, J.M., 2008. The effect of particle design on cellular internalization pathways. Proc. Natl. Acad. Sci. U.S.A. 105, 11613–11618.
Hirakawa, K., Suzuki, H., Oikawa, S., Kawanishi, S., 2003. Sequence-specific DNA damage induced by ultraviolet A-irradiated folic acid via its photolysis product. Arch. Biochem. Biophys. 410, 261–268.
John, G., Masuda, M., Okada, Y., Yase, K., Shimizu, T., 2001. Nanotube formation from renewable resources via coiled nanofibers. Adv. Mater. 13, 715–718.
Johnston, M.J., Semple, S.C., Klimuk, S.K., Edwards, K., Eisenhardt, M.L., Leng, E.C., Karlsson, G., Yanko, D., Cullis, P.R., 2006. Therapeutically optimized rates of drug release can be achieved by varying the drug-to-lipid ratio in liposomal vincristine formulations. Biochim. Biophys. Acta 1758, 55–64.
Kajiwara, E., Kawano, K., Hattori, Y., Fukushima, M., Hayashi, K., Maitani, Y., 2007. Long-circulating liposome-encapsulated ganciclovir enhances the efficacy of HSV-TK suicide gene therapy. J. Control. Release 120, 104–110.
Kamen, B.A., Caston, J.D., 1986. Properties of a folate binding protein (FBP) isolated from porcine kidney. Biochem. Pharmacol. 35, 2323–2329.
Kameta, N., Masuda, M., Shimizu, T., 2005. Selective construction of supramolecular nanotube hosts with cationic inner surfaces. Adv. Mater. 17, 2732–2736.
Kameta, N., Masuda, M., Minamikawa, H., Mishima, Y., Yamashita, I., Shimizu, T., 2007. Functionalizable organic nanochannels based on lipid nanotubes; encapsulation and nanofluidic behavior of biomacromolecules. Chem. Mater. 19, 3553–3560.
Kameta, N., Minamikawa, H., Masuda, M., Mizuno, G., Shimizu, T., 2008. Controllable biomolecule release from self-assembled organic nanotubes with asymmetric surfaces: pH and temperature dependence. Soft Matter 4, 1681–1687.
Kamiya, S., Minamikawa, H., Jung, J.H., Yang, B., Masuda, M., Shimizu, T., 2005. Molecular structure of glucopyranosylamide lipid and nanotube morphology. Langmuir 21, 743–750.
Kelemen, L.E., 2006. The role of folate receptor alpha in cancer development, progression and treatment: cause, consequence or innocent bystander? Int. J. Cancer 119, 243–250.

Kogiso, M., Zhou, Y., Shimizu, T., 2007. Instant preparation of self-assembled metal-complexed lipid nanotubes that act as self-templates to produce metal-oxide nanotubes. Adv. Mater. 19, 242–246.
Kogiso, M., Aoyagi, M., Asakawa, M., Shimizu, T., 2010a. Highly efficient production of organic nanotubes with various surfaces and their application as adsorbents. Soft Matter 6, 4528–4535.
Kogiso, M., Aoyagi, M., Asakawa, M., Shimizu, T., 2010b. Semi-solid phase synthesis of metal-complexed organic nanotubes. Chem. Lett. 39, 822–823.
Leamon, C.P., Low, P.S., 1991. Delivery of macromolecules into living cells: a method that exploits folate receptor endocytosis. Proc. Natl. Acad. Sci. U.S.A. 88, 5572–5576.
Liu, Z., Sun, X., Nakayama-Ratchford, N., Dai, H., 2007. Supramolecular chemistry on water-soluble carbon nanotubes for drug loading and delivery. ACS Nano 1, 50–56.
Lu, Y., Low, P.S., 2002. Folate-mediated delivery of macromolecular anticancer therapeutic agents. Adv. Drug Deliv. Rev. 54, 675–693.
Medina-Kauwe, L.K., Xie, J., Hamm-Alvarez, S., 2005. Intracellular trafficking of non-viral vectors. Gene Ther. 12, 1734–1751.
Nakashima, N., Asakuma, S., Kim, J., Kunitake, T., 1984. Helical superstructures are formed from chiral ammonium bilayers. Chem. Lett. 10, 1709–1712.
Shimizu, T., Masuda, M., Minamikawa, H., 2005. Supramolecular nanotube architectures based on amphiphilic molecules. Chem. Rev. 105, 1401–1443.
Shimizu, T., 2006. Self-assembled lipid nanotube hosts: the dimension control for encapsulation of nanometer-scale guest substances. J. Polym. Sci. Part A: Polym. Chem. 44, 5137–5152.
Shimizu, T., 2008a. Self-assembled organic nanotubes: toward attoliter chemistry. J. Polym. Sci. Part A: Polym. Chem. 46, 2601–2611.
Shimizu, T., 2008b. Molecular self-assembly into one-dimensional nanotube architectures and exploitation of their functions. Bull. Chem. Soc. Jpn. 81, 1554–1566.
Wattiaux, R., Laurent, N., Wattiaux-De, C.S., Jadot, M., 2000. Endosomes, lysosomes: their implication in gene transfer. Adv. Drug Deliv. Rev. 41, 201–208.
Yager, P., Schoen, P.E., 1983. Formation of tubules by a polymerizable surfactant. Mol. Cryst. Liq. Cryst. 106, 371–381.
Yamada, K., Ihara, H., Ide, T., Fukumiti, T., Hirayama, C., 1984. Formation of helical super structure from single-walled bilayers by amphiphiles with oligo-L-glutamic acid-head group. Chem. Lett. 10, 1713–1716.
Yang, B., Kamiya, S., Yoshida, K., Shimizu, T., 2004a. Confined organization of Au nanocrystals in glycolipid nanotube hollow cylinders. Chem. Commun. 2004, 500–501.
Yang, B., Kamiya, S., Shimizu, Y., Koshizaki, N., Shimizu, T., 2004b. Glycolipid nanotube hollow cylinders as substrates: fabrication of one-dimensional metallic-organic nanocomposites and metal nanowires. Chem. Mater. 16, 2826–2831.
Yokoyama, M., Okano, T., Akurai, Y., Kimoto, H., Hibazaki, C., Kataoka, K., 1991. Toxicity and antitumor activity against solid tumors of micelle-forming polymeric anticancer drug and its extremely long circulation in blood. Cancer Res. 51, 3229–3236.
Yui, H., Shimizu, Y., Kamiya, S., Masuda, M., Yamashita, I., Ito, K., Shimizu, T., 2005. Encapsulation of ferritin within a hollow cylinder of glycolipid nanotubes. Chem. Lett. 34, 232–233.

molecular pharmaceutics

ARTICLE

pubs.acs.org/molecularpharmaceutics

Octreotide-Targeted Liposomes Loaded with CPT-11 Enhanced Cytotoxicity for the Treatment of Medullary Thyroid Carcinoma

Yuko Iwase and Yoshie Maitani*

Institute of Medicinal Chemistry, Hoshi University, Ebara 2-4-41, Shinagawa, Tokyo 142-8501, Japan

Supporting Information

ABSTRACT: Medullary thyroid carcinoma (MTC) is a rare endocrine tumor that frequently metastasizes, but treatment with irinotecan (CPT-11) is limited because of side effects. MTC is known to overexpress the somatostatin receptor subtype 2 (SSTR2). Octreotide (Oct) is a somatostatin analogue that has a high binding affinity for SSTR and can be used as a tumor-targeting ligand. We prepared Oct-targeted liposomes loaded with CPT-11 using Oct-poly (ethylene glycol) (PEG)-lipid and evaluated Oct-mediated association and cytotoxicity of the liposomes with an MTC cell line TT. The association of higher concentrations of modified Oct-targeted liposomes with TT cells was significantly higher than PEGylated liposomes and was significantly inhibited by empty Oct-targeted liposomes but not by free Oct. With exposure for 96 h, the cytotoxicity of Oct-targeted liposomal CPT-11 (IC50: 1.05 ± 0.47 μM) was higher than free CPT-11 (IC50: 3.76 ± 0.61 μM) or PEGylated liposomal CPT-11 (IC50: 3.05 ± 0.28 μM). In addition, empty Oct-targeted liposomes showed significantly higher cytotoxicity than empty nontargeted liposomes at a concentration where free Oct did not show cytotoxicity, suggesting that Oct as a ligand showed cytotoxicity. Moreover, Oct-targeted liposomal CPT-11 led to significantly higher antitumor activity and prolonged the survival time compared with nontargeted liposomal and free CPT-11 at a one-third dose and lower administration times with free CPT-11. These findings indicated that Oct-targeted liposomes loaded with CPT-11 may offer considerable potential for MTC chemotherapy because cytotoxicity of both CPT-11 and Oct was enhanced by effective cellular uptake *via* SSTR2.

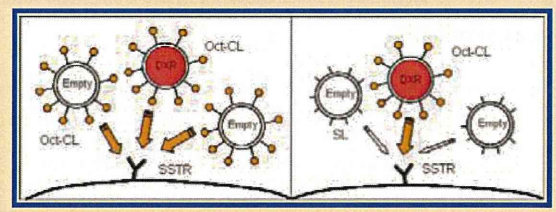

KEYWORDS: octreotide, CPT-11, medullary thyroid carcinoma, somatostatin receptor, targeting liposome, antitumor activity

1. INTRODUCTION

Medullary thyroid carcinoma (MTC) is a rare endocrine tumor comprising a malignant neoplasm of calcitonin-secreting C cells of the thyroid and represents approximately 3−5% of all thyroid cancers.[1] MTC occurs in a sporadic form in about 75% of cases, and the remaining 25% are three familial forms: multiple endocrine neoplasia type IIA (MEN 2A), multiple endocrine neoplasia type IIB (MEN2B), and familial MTC not associated with MEN (FMTC).[2] The only effective treatment for MTC is surgical removal of the neoplastic tissue with central lymph node dissection.[3] In the case of total thyroidectomy, however, life-long hormone replacement therapy is necessary for the patient. Most chemotherapy or radiotherapy for MTC has inconclusive results. The lack of effective systemic therapy for MTC shows the importance of developing new approaches for the treatment of MTC.

Recently, therapeutic approaches for MTC using irinotecan (CPT-11) have been reported.[4,5] CPT-11 is a water-soluble derivative of camptothecin and is converted to SN-38, the active form of CPT-11, by carboxyl esterase.[6,7] CPT-11 inhibits the resealing of single-strand DNA breaks mediated by topoisomerase I by stabilizing cleavable complexes and is a cell-cycle-specific drug.[8−10] Based on this, a long period of exposure to CPT-11 mediates a reduction in tumor cells, but treatment with CPT-11 is limited because of its short half-life and serious side effects, such as bone-marrow suppression.[11] Success in the treatment of MTC with CPT-11 requires selective delivery to tumor tissues and limited distribution to normal tissues.

For this purpose, liposomal CPT-11 could be advantageous. Liposomal drugs reduce renal clearance and, when formulated for long circulation, may increase accumulation of the drug in a tumor by a passive targeting process based on the enhanced permeability and retention (EPR) effect in leaky tumor tissue. To further enhance the therapeutic effects of liposomal drugs in tumors, a variety of targeting ligands have been investigated. Somatostatin receptors (SSTRs) belong to a seven-transmembrane domain G-protein coupled receptor family (SSTR1, SSTR2, SSTR3, SSTR4, and SSTR5)[12] and can serve as a functional tumor-specific receptor. MTC tumors express all the SSTR subtypes, and the MTC cell line TT overexpresses SSTR1, SSTR2 and SSTR5.[13] SSTR2 expression was significantly higher than the other SSTR subtypes in TT cells and was the most

Received: May 11, 2010
Accepted: December 17, 2010
Revised: December 9, 2010

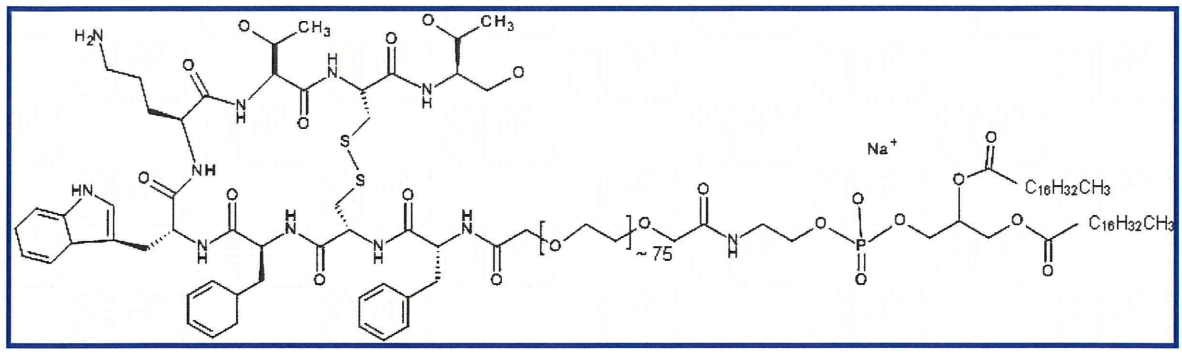

Figure 1. Chemical structure of Oct-PEG_{3400}-DSPE (MW = ~5200).

frequently detected subtype in human MTC.[13−15] Octreotide (Oct) has high binding affinity to all SSTR subtypes,[16] especially SSTR2 (affinity 0.56 nM).[12] Oct is an octapeptide analogue of natural somatostatin with markedly increased metabolic stability,[17] resulting in an increased plasma-half-life of >1 h in rats[17] and humans.[18] Oct has been marketed as a diagnostic agent.[19−21] It was reported that Oct-modified particles loaded with anticancer drugs (cantharidin and dihydrotanshinone I) were efficacious in breast cancer and gastric cancer, respectively.[22,23] To the best of our knowledge, this report is the first to explore the use of Oct-targeted liposomes for the treatment of MTC.

Here, we hypothesized that Oct-targeted liposomal CPT-11 could enable selective delivery of CPT-11 and increase the therapeutic efficacy of CPT-11 for MTC. Previously, we succeeded in preparing liposomes with a high loading efficacy for CPT-11.[24] In this study, we prepared Oct-targeted liposomes loaded with CPT-11 and evaluated the Oct-mediated association and therapeutic potential of Oct-targeted liposomes with TT cells and TT tumor xenografts in mice, for the comparison of free and liposomal CPT-11.

2. MATERIALS AND METHODS

2.1. Materials

2.1.1. Materials. CPT-11 was a kind gift from Yakult Co., Ltd. (Tokyo, Japan). Oct-poly(ethylene glycol)$_{3400}$-distearoylphosphatidylethanolamine (Oct-PEG_{3400}-DSPE)[25] was purchased from KNC Laboratories. Co., Ltd. (Kobe, Japan) (Figure 1). Oct was purchased from Acris Antibodies GmbH (Herford, Germany). Distearoylphosphatidylcholine (DSPC) and methoxy-PEG_{2000}-DSPE (PEG_{2000}-DSPE) were purchased from the NOF Corp. (Tokyo, Japan). Cholesterol, doxorubicin (DXR) hydrochloride, and Ham's F-12 medium were purchased form Wako Pure Chemical Industries, Ltd. (Osaka, Japan). Phytic acid (IP-6) solution was obtained from Nacalai Tesque Inc. (Kyoto, Japan). Fetal bovine serum (FBS) was purchased from Invitrogen Corp. (Carlsbad, CA, USA). Nonessential amino acids were purchased from MP Biomedicals (Cleveland, OH, USA). Other reagents were of analytical or HPLC grade.

2.1.2. TT Cell Line Culture. The TT cell was obtained from the European Collection of Cell Cultures (ECACC, Wiltshire, UK). This cell line was routinely maintained in Ham's F-12 medium supplemented with 10% heat-inactivated FBS at 37 °C in a humidified atmosphere containing 5% CO_2.

2.2. Preparation of Oct-Targeted Liposomes Loaded with Drug

2.2.1. Preparation of Liposomal CPT-11 and DXR. Liposomes containing IP-6 (IP-6 liposomes) were formulated following previously described methods.[24] Briefly, DSPC and cholesterol at a molar ratio of 55:45 (80 mg/32 mg) were dissolved in ethanol. Ethanol was removed by rotary evaporation to a smaller volume, and 80 mM IP-6 solution adjusted to pH 6.5 using triethanolamine was added immediately, followed by sonication to decrease the size to approximately 150 nm. Then, the extra liposomal IP-6 suspension was exchanged for HBS buffer (20 mM HEPES, 150 mM NaCl, pH 7.4) by gel filtration chromatography using a Sephadex G50 column. The concentration of phospholipid (DSPC) of IP-6 liposomes was determined using a phospholipid C Test Wako (Wako Pure Chemical Industries, Ltd.), and then total lipid was calculated using DSPC and cholesterol at a molar ratio of 55:45. IP-6 liposomes were loaded with DXR or CPT-11 by incubation with CPT-11 (drug:total lipid = 0.6:1, w/w) at 60 °C for 60 min or with DXR (drug:total lipid =0.2:1, w/w) at 60 °C for 25 min, and then quenched in ice for 5 min. Unincorporated CPT-11 or DXR was removed using a Sephadex G-50 column eluted with saline as the mobile phase.

2.2.2. Modification of Liposomal Drug with Oct. Three types of liposomes were prepared: conventional non-PEGylated and nontargeted liposomes (CL), Oct-targeted liposomes (Oct-CL), and PEGylated, sterically stabilized liposomes (SL). Oct-CL was prepared by incubation of CL with an aqueous dispersion of 0.25−1.6 mol % Oct-PEG-DSPE with total lipids at 60 °C for 20 min by the postinsertion technique as reported previously.[26] Above 1.6 mol %, Oct-PEG-DSPE precipitates because of its insolubility in water. SL was prepared by incubation of CL with aqueous dispersion of 1.6 mol % PEG-DSPE in total lipids. CL modified with x mol % Oct-PEG-DSPE of total lipids are henceforth abbreviated as xOct-CL. For example, 0.25Oct-CL indicates liposomes with 0.25 mol % Oct-PEG-DSPE in total lipids (Table 1). Empty liposomes were prepared using the same protocol but without loading drug.

The mean diameter and zeta-potential of the resulting liposomes were determined using a ELS-Z2 (Otsuka, Electronics CO., Ltd. Osaka, Japan) at 25 ± 1 °C after diluting the liposome suspension with water. Drug concentration in the liposomes was determined after disruption of liposomes using 1% of Triton; DXR was determined using a UV-1700 PharmaSpec (Shimadzu, Kyoto, Japan) at 480 nm[26] and CPT-11 using a fluorometer (excitation wavelength 355 nm and emission wavelength 535 nm, Wallac ARVO SX1420 multilabel counter, PerkinElmer Japan, Yokohama, Japan).[24] No drug leaked out from the liposomes during the Oct-PEG-DSPE insertion procedure. The final Oct concentration after modification of the liposomes was determined using an Oct-EIA kit (Peninsula Laboratories, LLC, San Carlos, CA, USA) after disruption of the liposomes by dilution